Article

Immunity

Regulatory T Cell Migration Is Dependent on Glucokinase-Mediated Glycolysis

Graphical Abstract

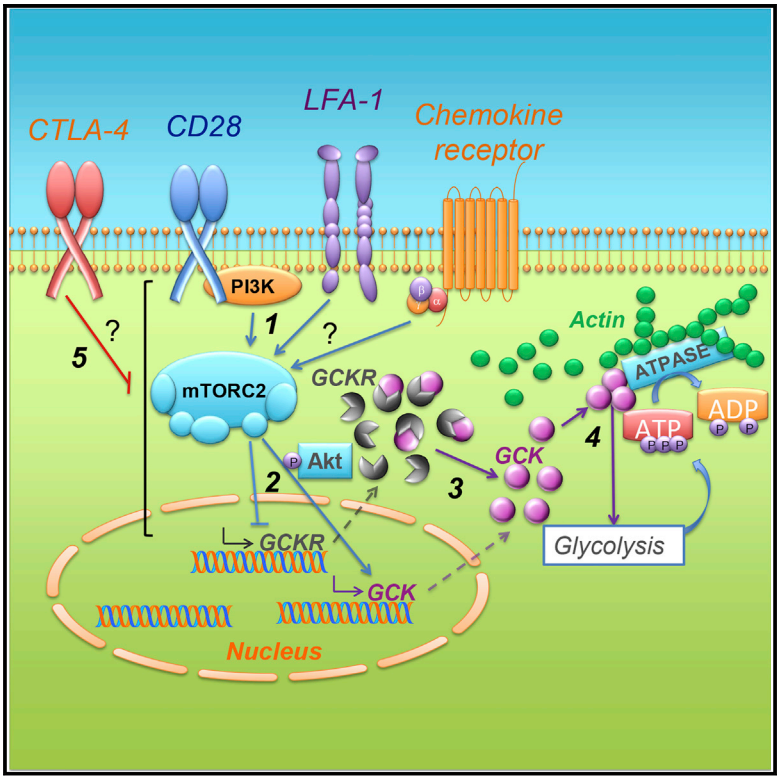

Highlights

- Migration of regulatory T (Treg) cells requires glycolysis
- This is mediated by the enzyme glucokinase induced by a PI3K-mTORC2 pathway
- Treg cells lacking this pathway are unable to localize to inflammatory sites
- A loss-of-function GCK regulator gene causes enhanced motility of human Treg cells

Authors

Madhav Kishore, Kenneth C.P. Cheung, Hongmei Fu, ..., Veronica De Rosa, Giuseppe D. Norata, Federica M. Marelli-Berg

Correspondence

f.marelli-berg@qmul.ac.uk

In Brief

Regulatory T cell localization to inflammatory sites is key to their homeostatic function. Kishore and colleagues demonstrate that Treg cell migration requires the activation of glycolysis by the enzyme glucokinase induced via a Treg cell-selective PI3K-mTORC2 pathway.

Kishore et al., 2017, Immunity *47*, 875–889
November 21, 2017
https://doi.org/10.1016/j.immuni.2017.10.017

CellPress

Immunity
Article

Regulatory T Cell Migration Is Dependent on Glucokinase-Mediated Glycolysis

Madhav Kishore,[1,10] Kenneth C.P. Cheung,[1,10] Hongmei Fu,[1,11] Fabrizia Bonacina,[2,11] Guosu Wang,[1] David Coe,[1] Eleanor J. Ward,[1] Alessandra Colamatteo,[3] Maryam Jangani,[1] Andrea Baragetti,[2] Giuseppe Matarese,[3,4] David M. Smith,[5] Robert Haas,[1] Claudio Mauro,[1] David C. Wraith,[6] Klaus Okkenhaug,[7] Alberico L. Catapano,[2,8] Veronica De Rosa,[3,12] Giuseppe D. Norata,[2,9,12] and Federica M. Marelli-Berg[1,13,*]

[1]William Harvey Research Institute, Queen Mary University of London, London EC1M6BQ, UK
[2]Department of Pharmacological and Biomolecular Sciences, University of Milan, Milan 20133, Italy
[3]Istituto per l'Endocrinologia e l'Oncologia Sperimentale, Consiglio Nazionale delle Ricerche (IEOS-CNR), Naples 80131, Italy
[4]Dipartimento di Medicina Molecolare e Biotecnologie Mediche, Università di Napoli "Federico II," Naples 80131, Italy
[5]Discovery Sciences, Innovative Medicines and Early Development Biotech Unit, AstraZeneca, Cambridge, Cambridgeshire CB40WG, UK
[6]Institute of Immunology and Immunotherapy, University of Birmingham, Birmingham B15 2TT, UK
[7]Laboratory of Lymphocyte Signalling and Development, Babraham Institute, Cambridge CB22 3AT, UK
[8]IRCCS Multimedica Hospital, Milan 20138, Italy
[9]School of Biomedical Sciences, Curtin Health Innovation Research Institute, Curtin University, Perth, WA 6102, Australia
[10]These authors contributed equally
[11]These authors contributed equally
[12]Senior author
[13]Lead Contact
*Correspondence: f.marelli-berg@qmul.ac.uk
https://doi.org/10.1016/j.immuni.2017.10.017

SUMMARY

Migration of activated regulatory T (Treg) cells to inflamed tissue is crucial for their immune-modulatory function. While metabolic reprogramming during Treg cell differentiation has been extensively studied, the bioenergetics of Treg cell trafficking remains undefined. We have investigated the metabolic demands of migrating Treg cells *in vitro* and *in vivo*. We show that glycolysis was instrumental for their migration and was initiated by pro-migratory stimuli via a PI3K-mTORC2-mediated pathway culminating in induction of the enzyme glucokinase (GCK). Subsequently, GCK promoted cytoskeletal rearrangements by associating with actin. Treg cells lacking this pathway were functionally suppressive but failed to migrate to skin allografts and inhibit rejection. Similarly, human carriers of a loss-of-function GCK regulatory protein gene—leading to increased GCK activity—had reduced numbers of circulating Treg cells. These cells displayed enhanced migratory activity but similar suppressive function, while conventional T cells were unaffected. Thus, GCK-dependent glycolysis regulates Treg cell migration.

INTRODUCTION

Thymic regulatory T (Treg) cells, defined as $CD4^+CD25^+Foxp3^+$ T cells, are instrumental for the maintenance of tolerance to self-antigens. Treg cells exert their immunomodulatory role by localizing to both lymphoid and non-lymphoid tissue.

A rapid accumulation of Treg cells relative to T effector (Teff) cells—in which more than 30% of the infiltrating lymphocytes are Treg cells—occurs in inflamed tissue during immune regulation (Tang et al., 2012). By contrast, the small proportion of these cells in the peripheral blood (2%–5%) further emphasizes their remarkable migratory ability.

The bioenergetics of Teff and Treg cell function, expansion, and survival has been extensively studied. Teff and Treg cells require distinct metabolic programs to support their survival and differentiation: T helper (Th)1, Th2, and Th17 cells express high surface amounts of glucose transporter Glut1 and are highly glycolytic, whereas Treg cells express low amounts of Glut1 and have high lipid oxidation rates *in vitro* (Michalek et al., 2011). The mammalian target of rapamycin (mTOR) plays a key role in cell fate decision by regulating T cell metabolic responses. T cell activation stimulates mTOR to increase glycolysis and diminish lipid oxidation (Wieman et al., 2007). In contrast, blockade of glycolysis promotes generation of Treg cells, and this occurs via inhibition of mTOR-mediated induction of the transcription factor hypoxia-inducible factor (HIF1α) (Dang et al., 2011; Shi et al., 2011). However, while Treg cells mainly rely upon an oxidative metabolism, some specific functions can be dependent on a selective switch to glycolysis. Their metabolism appears to oscillate from mTOR-dependent and -independent pathways in response to environmental cues (Procaccini et al., 2010). Toll-like receptor (TLR) signals promote Treg cell proliferation via mTORC1 signaling, glycolysis, and Glut1 upregulation, but these signals also reduce their suppressive ability (Gerriets et al., 2016).

Despite motility being likely the most energy-consuming cellular activity (Bernstein and Bamburg, 2003), the metabolic demands for T cell migration have been only partly investigated. We have shown that Teff cell migration relies upon the glycolytic pathway (Haas et al., 2015). However, the metabolic program(s) that fuel Treg cell migration remain unknown.

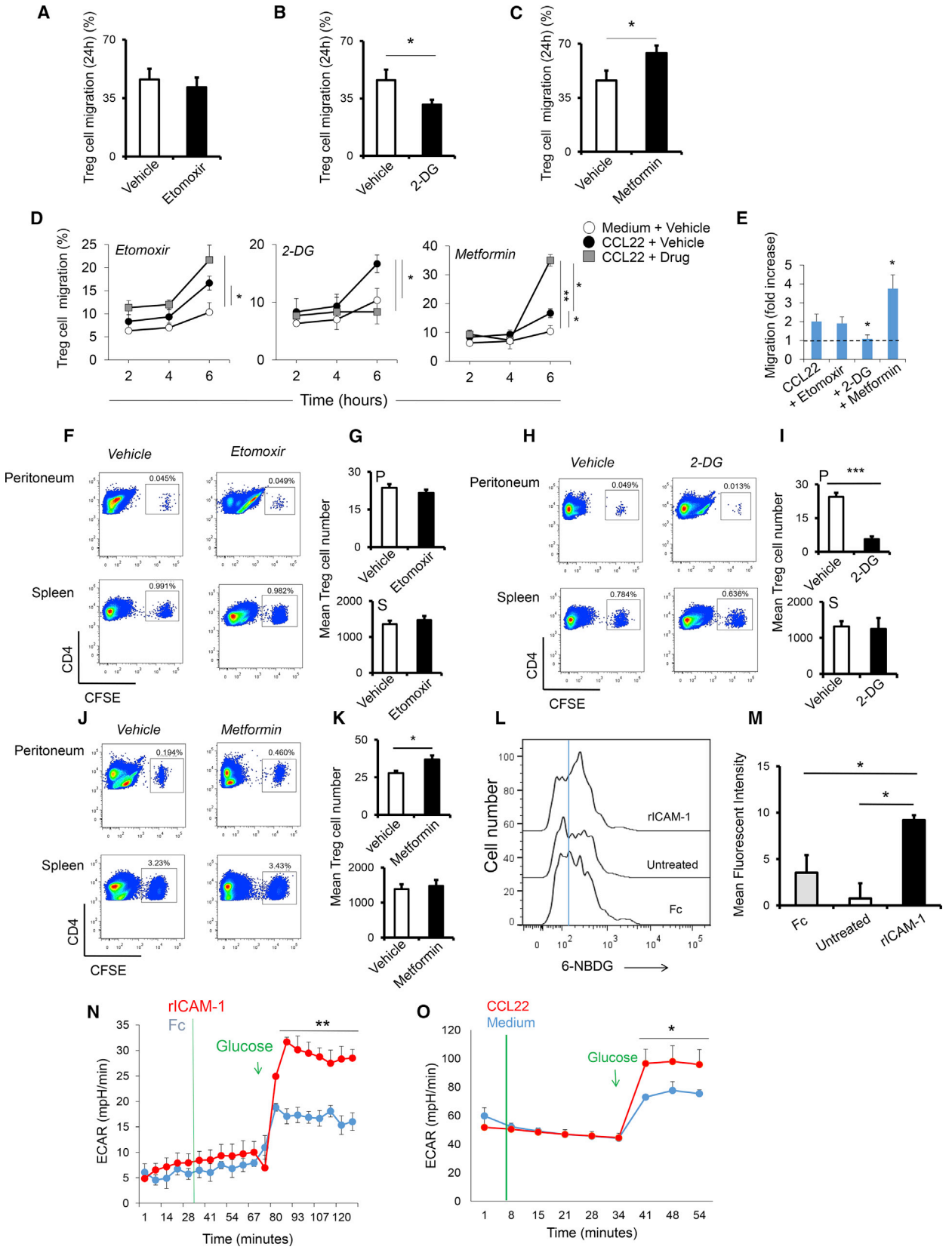

(legend on next page)

Integrins such as LFA-1 play a key role T cell trafficking; in addition, signals generated by the co-stimulatory or the co-inhibitory receptors CD28 and CTLA-4, respectively, actively participate in the regulation of T cell trafficking. In the lymph nodes, CD28 activation promotes memory T cell egression and migration to target tissue (Jain et al., 2013; Mirenda et al., 2007), while CTLA-4 antagonizes CD28 pro-migratory signals (Mirenda et al., 2007). Effector Treg cell migration is also regulated by CD28 signals (Müller et al., 2008). Importantly, costimulatory receptors also regulate T cell metabolic reprogramming to enhanced glycolysis (Frauwirth et al., 2002; Parry et al., 2005), suggesting that glycolysis and migration might be tightly linked in Treg cells.

By comparing LFA-1- and CD28-mediated pro-migratory signals as a working model, we have investigated the bioenergetics of migrating Treg cells *in vitro* and *in vivo*. We here define a specific pathway of metabolic reprogramming sustaining Treg cell migration both in mice and humans.

RESULTS

Engagement of the Glycolytic Pathway Is Required for Treg Cell Migration

Given that Treg cells display high lipid oxidation, we first tested the hypothesis that *ex vivo* expanded thymic Treg cell migration may require fatty acid oxidation (FAO) by exposing the cells to acetyl-CoA carboxylase (ACC) inhibitor Etomoxir (Figures S1B and S1C). This pre-treatment did not affect Treg cell transendothelial migration (TEM) or chemotaxis *in vitro* (Figures 1A, 1D, and 1E, respectively, and S1A–S1E) or migration to inflamed peritoneum *in vivo* (Figures 1F and 1G).

We subsequently explored the possibility that, like conventional T cells (Tconv), Treg cells utilize glycolysis for migration, by inhibiting this pathway with the glucose analog 2-deoxyglucose (2-DG). Treg cells exposed to 2-DG migrated inefficiently both *in vitro* (Figures 1B, 1D, 1E, S1D, and S1E) and *in vivo* (Figures 1H and 1I). In addition to extensive washing after exposure to the drugs, the inhibition of Treg cell chemotaxis excludes indirect effects of the drugs on the endothelium in these conditions. In contrast, activation of glycolysis using metformin, which stimulates glycolysis via AMP kinase, increased Treg cell motility (Figures 1C–1E, S1D, and S1E) and trafficking (Figures 1J and 1K). None of the drugs affected expression of migration-relevant receptors or viability at the doses used (Figures S1F and S1G). To confirm that the effect of each of these compounds is retained once *in vitro* treated T cells are injected into recipient mice, Treg cells were exposed to the various drugs for 4 hr, extensively washed, and incubated in culture medium alone for a further 16 hr. The effects on drug-treated cell motility were still apparent after the prolonged incubation without the compounds (Figures S1I–S1N).

To confirm the induction of the glycolytic pathway by pro-migratory stimuli, we subsequently tested the effect of engagement of the adhesion molecule integrin LFA-1, a key mediator of T cell migration, on aerobic glycolysis in Treg cells. Immobilized or antibody-ligated recombinant mouse ICAM-1 (rICAM-1), a ligand of LFA-1, was used for this purpose.

First we estimated LFA-1-induced glucose uptake using the glucose analog 6-[N-(7-nitrobemz-2-oxa-1,3-diazol-4-yl) amino]-2-deoxyglucose (6-NBDG), which cannot be phosphorylated by hexokinases and accumulates in the cytoplasm in its fluorescent form. Treg cells were stimulated with plastic-bound rICAM-1 or human IgG Fc fragments (control) and 6-NBDG uptake was measured 30 min later by flow cytometry. As shown in Figures 1L and 1M, LFA-1 stimulation significantly increased 6-NBDG uptake.

Second, we measured the effects of LFA-1 engagement or exposure to the chemokine CCL22 (CCR4 ligand) on the extracellular acidification rate (ECAR), which quantifies proton production as a surrogate for lactate production and thus reflects overall glycolytic flux. ECAR increase upon glucose supply was significantly enhanced following LFA-1 or CCR4 (Figures 1N and 1O) stimulation. Meanwhile, the oxygen consumption rate (OCR), a measure of mitochondrial respiration, was not affected (Figures S1N and S1O).

CD28 and CTLA-4 Regulate Treg Cell Migration through Modulation of the Glycolytic Pathway

As triggering of LFA-1 by endothelial ICAM-1 is a frequent event during recirculation—hence difficult to manipulate—to address the metabolic requirement of Treg cell trafficking *in vivo* we subsequently focused on the effects CD28 and CTLA-4 (Figure S2A) costimulatory and coinhibitory signals, which can be delivered *ex vivo* with well-characterized reagents (Figure S2B).

First, we confirmed that antibody activation of CD28 enhances *ex vivo* expanded Treg cell TEM (Figure S2C) and chemotaxis (Figures S2D and S2E) *in vitro* and migration *in vivo* (Figure S2F), without affecting expression of relevant receptors (Figures S2G and S2H). Also, we observed that while CTLA-4 triggering alone did not affect cell migration, co-ligation with CD28 abrogated CD28-induced migration (Figures S2C and S2D).

Figure 1. Glycolysis Fuels Treg Cell Migration

(A–E) *Ex vivo* expanded Treg cells pre-treated with the indicated drugs or vehicle for 4 hr were left to migrate through 3 μm-pore transwells layered with IFN-γ-treated syngeneic EC monolayers (A–C) or in response to chemokine CCL22 through bare-filter 5 μm-pore transwells (D and E). Results are expressed as percentage of migrated cells after 24 hr (A–C, n = 4, N = 2) or at the indicated time points (D, n = 3) ± SD. The fold increase in migration was calculated by dividing experimental migration by spontaneous migration measured at 6 hr in two experiments of identical design performed in triplicates ± SD.

(F–K) Drug- or vehicle-treated Treg cells labeled with PKH26 were injected i.v. into syngeneic recipients treated with IFN-γ i.p. 48 hr earlier. Cells were harvested from the indicated tissues after 24 hr and analyzed by flow cytometry. Representative dot plots from 3 animals are shown in (F), (H), and (J). The mean absolute number of labeled cells recovered in 4 animals ± SD is shown in (G), (I), and (K) (N = 1).

(L and M) Representative histograms from 3 independent experiments of Treg cells stimulated with plastic-bound recombinant (r)ICAM-1 or human IgG Fc fragments (Fc) for 45 min and then re-suspended in medium containing the glucose uptake indicator 6-NBDG for 10 min. The mean MFI ± SD is shown in (M).

(N and O) ECAR of ICAM-1- (N) or CCL22-stimulated (O) cells was measured by an extracellular flux analyzer (Seahorse). Ig Fc or medium was used as a control. Recombinant molecules and glucose were added at the time points indicated (±SD n = 5, N = 2).

*p < 0.05, **p < 0.005. Please see also Figure S1.

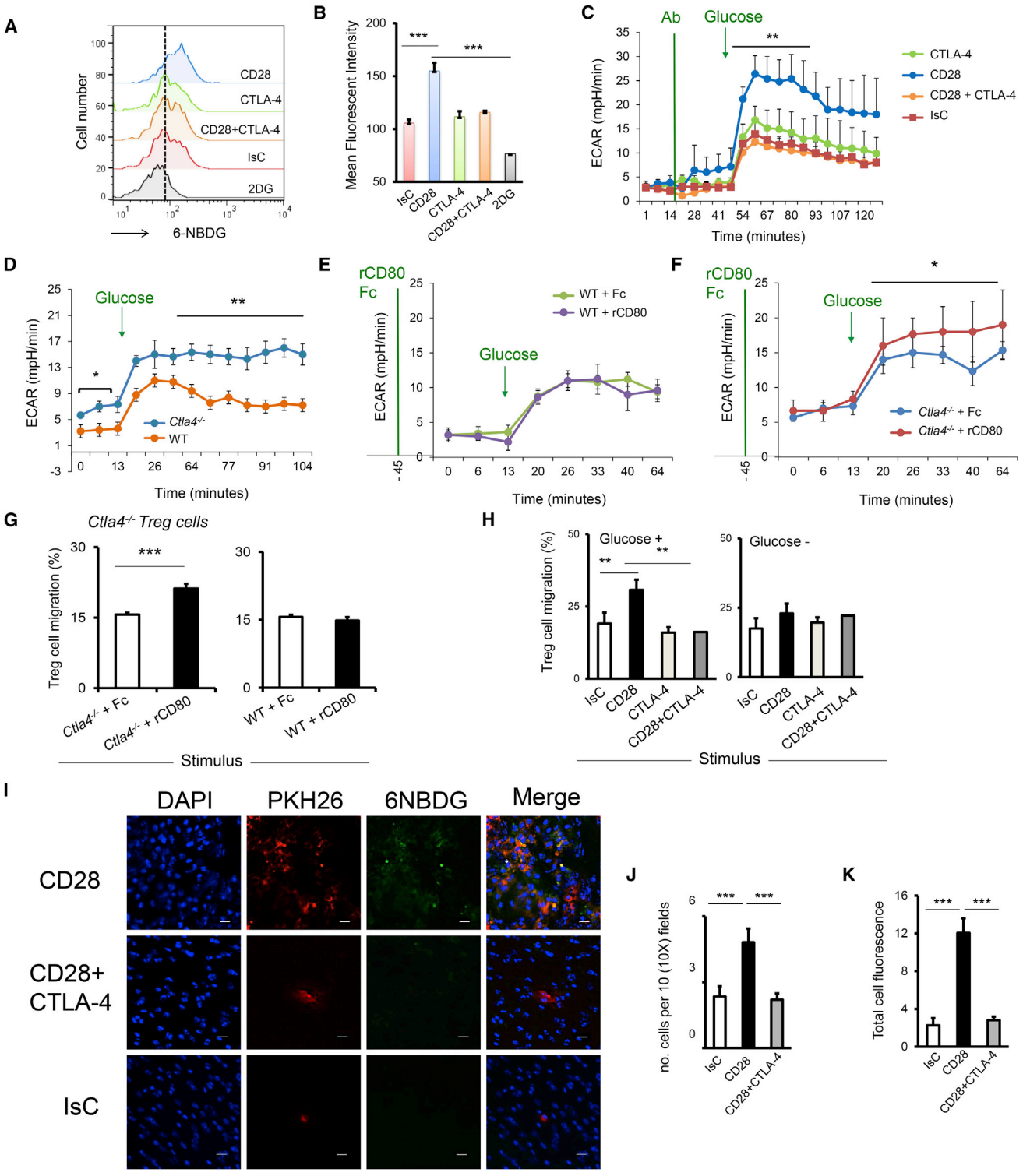

Figure 2. Treg Cell Migration Is Regulated by Co-stimulatory Receptors via Induction of Glycolysis

(A and B) Representative histograms from 3 independent experiments of antibody-stimulated Treg cells incubated with 6-NBDG for 10 min prior to analysis. The non-fluorescent glucose analog 2-DG was used as a negative control. The mean MFI ± SD is shown in (B) (N = 3).

(C) ECAR of antibody-stimulated Treg cells was measured by fluxometry. Antibodies (Ab) and D-glucose were injected at the indicated time points ± SD.

(D–F) ECAR (±SD) was measured in WT or *Ctla4*$^{-/-}$ Treg cells either unstimulated (D) or previously stimulated with recombinant CD80 or Fc fragments for 30 min (E and F). D-glucose was injected as indicated by the green line.

(legend continued on next page)

Second, we measured the impact of CD28 and CTLA-4 signals on the glycolytic pathway in Treg cells. CD28 triggering significantly increased 6-NBDG uptake (Figures 2A and 2B) and glycolytic flux (Figure 2C) compared to treatment with an isotype control and secondary antibodies. In contrast, CTLA-4 stimulation did not affect either glucose uptake or ECAR on its own but when co-ligated, CTLA-4 signals prevented CD28-induced glucose uptake and ECAR increase. The oxygen consumption rate (OCR) was not affected by triggering of either costimulatory receptor (Figures S2I and S2J).

We further explored the link between costimulatory signals and metabolic regulation of motility by analyzing the metabolic activity and migration of *Ctla4*$^{-/-}$ Treg cells. In these experiments we used as stimulator recombinant (r)CD80, a ligand shared by CD28 and CTLA-4. Compared to WT Treg cells, *Ctla4*$^{-/-}$ cells displayed a prolonged increase of ECAR in response to glucose (Figure 2D)—even taking into account a higher acidification baseline. As expected, the ECAR of WT Treg cells activated with recombinant CD80 remained unchanged, due to simultaneous CD28 and CTLA-4 engagement (Figure 2E), while *Ctla4*$^{-/-}$ cells further increased their glycolytic response to glucose addition (Figure 2F). Despite the fact that *Ctla4*$^{-/-}$ cell OCR was spontaneously higher than that of their WT counterparts, it was not affected by either CD28 or CTLA-4 signals (Figure S2K).

In parallel, we tested TEM by rCD80-stimulated *Ctla4*$^{-/-}$ Treg cells through IFN-γ-activated syngeneic EC. As shown in Figure 2G, *Ctla4*$^{-/-}$ Treg cell stimulated with recombinant CD80 displayed enhanced migration through EC while WT Treg cells did not respond to such stimulation, supporting the conclusion that CTLA-4 signals inhibit CD28-induced glycolysis and migration.

To investigate whether control of Treg cell migration by CD28 and CTLA-4 occurs via modulation of glycolysis, we analyzed the effect of CD28 and/or CTLA-4 stimulation during TEM in glucose-depleted medium. As shown in Figure 2H, glucose depletion prevented the increase in motility induced by CD28 signals. The results were not influenced by cell distress associated with glucose deprivation as baseline migration remained similar in both glucose-sufficient and -deficient conditions.

In vivo, the CD28-glycolysis-migration axis was analyzed by monitoring 6-NBDG uptake by CD28-stimulated migrating Treg cells. To this aim, we used a tissue infiltration model in which the ability of Treg cells injected in the peritoneal cavity to infiltrate the peritoneal membrane is quantified (Mirenda et al., 2007). This model was chosen because 6-NBDG fluorescence is rapidly lost with time, making it technically impossible to track T cells transferred intravenously long-term. Treg cells were labeled with PKH26 (red fluorescence) and then underwent CD28 ligation with or without CTLA-4 triggering, or received isotype-matched and secondary antibodies as a control prior to i.p. injection in syngeneic mice treated with IFN-γ 48 hr earlier. 6-NBDG (green fluorescence) was injected i.p. immediately after the cells, thus allowing parallel evaluation of tissue infiltration and glucose uptake by labeled Treg cell *in vivo*. As shown in Figures 2I–2K, CD28 activation substantially increased the number of cells infiltrating the peritoneum and displaying 6-NBDG uptake (yellow fluorescence), indicating that Treg cell migration directly correlates with glucose uptake *in vivo*. Both these effects were prevented by CTLA-4 co-ligation.

Enhancement of Glycolysis and Migration Requires PI3K-Akt Activation but Is Independent of mTORC1

CD28 stimulation induces glucose uptake and glycolysis via activation of the PI3K-Akt signaling pathway (Frauwirth et al., 2002; Jacobs et al., 2008). PI3K activation by CD28 is instrumental for the transduction of pro-migratory signals, without affecting expression of migratory receptors, in conventional T (Tconv) cells (Jarmin et al., 2008), and inefficient migration of T cells to the inflammatory site is a feature of *Cd80*$^{-/-}$*Cd86*$^{-/-}$ mice (Chang et al., 1999). To investigate the role of CD28-induced activation of the PI3K pathway on Treg cell metabolism and migration, we isolated Treg cells from *Cd28*^{Y170F} genetically targeted mice, which carry a mutation in the cytoplasmic tail of CD28 that selectively prevents recruitment of PI3K (Okkenhaug et al., 2001). *Cd28*^{Y170F} Treg cells display normal development (Tai et al., 2005) and expression of migration-relevant and other receptors (Figure S3A).

First, we compared the mobilization and recirculation of WT and *Cd28*^{Y170F} Treg cells following i.p. injection of Zymosan. Activation of innate but not adaptive immunity by this method has been shown to induce accumulation of Treg cells in the peritoneal cavity with a peak 72 hr after injection (Newson et al., 2014). As shown in Figures 3A and 3B, WT and *Cd28*^{Y170F} Treg cells—identified as shown in Figure S3B—increased in the peripheral blood to similar amounts by 72 hr after Zymosan injection. However, *Cd28*^{Y170F} Treg cells did not efficiently migrate to the peritoneal cavity and lymph nodes, indicative of inadequate extravasation from the bloodstream. CD28 is likely to be engaged during interactions with LPS-activated dendritic cells. The ratio of WT Treg cells in LN and blood and in blood and peritoneum decreased over time, indicating a LN-to-blood-to-peritoneum recirculation (Figures 3C and 3D). In contrast, the distribution of *Cd28*^{Y170F} Treg cells remained stable, confirming their impaired recirculation and additionally suggesting that the increase of these cells in the blood is likely due to passive mobilization from the spleen. Thus, CD28 instructs Treg cell recirculation in response to activation of innate immunity.

We subsequently compared the ECAR of CD28-stimulated purified *Cd28*^{Y170F} and WT Treg cells. After glucose addition,

(G) Migration of rCD80- or Fc-stimulated *Ctla4*$^{-/-}$ and WT Treg cells through syngeneic IFN-γ-treated EC monolayers. Results are expressed as mean percentage of migrated cells at 24 hr ± SD n = 3, N = 4.

(H) Migration of antibody-stimulated Treg cells re-suspended in either glucose-free or glucose-reconstituted medium through IFN-γ-treated syngeneic EC monolayers, expressed as percentage of migrated cells after 24 hr ± SD (n = 3, N = 4).

(K) Antibody-stimulated Treg cells labeled with PKH26 (red) were injected i.p. in C57BL/6 mice given IFN-γ i.p. 48 hr earlier. 6-NBDG (green) was injected i.p. immediately after. Peritoneal membranes were removed 1 hr later, counterstained with DAPI and imaged by wide-field fluorescence microscopy to determine the number of infiltrating cells and 6-NBDG uptake by the infiltrating cells. Representative images from 2 independent experiments are shown in (I). The mean number of cells counted in 10 10× fields from 4 recipients ± SD and the mean total cell fluorescence of 6-NBDG from 10–12 cells from 3 10× fields ± SD are shown in (J) and (K), respectively (n = 4, N = 2).

*p < 0.05; **p < 0.01; ***p < 0.005. Please see also Figure S2.

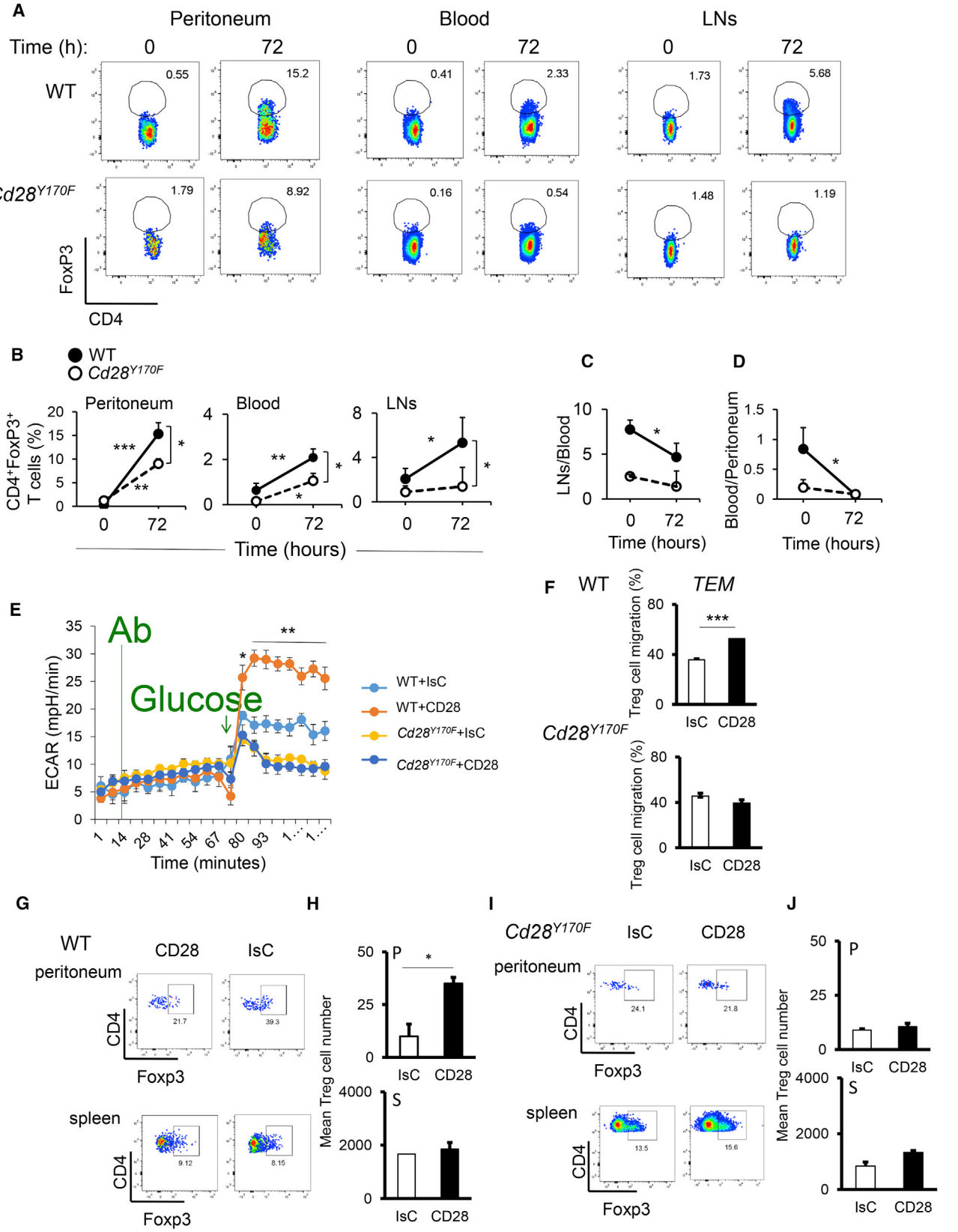

(legend on next page)

the ECAR increase in CD28-stimulated *Cd28*^{Y170F} cells was significantly dampened (Figure 3E), suggesting that PI3K recruitment by CD28 signals is required to efficiently induce glycolysis.

We then analyzed the migratory response to CD28 triggering by Treg cells isolated and expanded from both WT and *Cd28*^{Y170F} mice. As shown in Figures 3F–3J, CD28 stimulation failed to enhance migration of *Cd28*^{Y170F} Treg cells *in vitro* (Figure 3F) and *in vivo* (Figures 3G–3J), confirming the pivotal role of CD28-mediated recruitment of PI3K in enhancing Treg cell migration.

In most T lymphocytes, mTOR kinase couples upstream PI3K and Akt to glucose uptake and glycolysis (Chi, 2012; Powell and Delgoffe, 2010). In Treg cells, CD28 signals induced phosphorylation of the mTORC1 target ribosomal protein S6 (Figure S3C), an event that was prevented by CTLA-4 co-ligation. Rapamicyn treatment prevented Treg cells entering the cell cycle—as measured by the expression of the proliferating cell nuclear antigen (PCNA)—in response to immature cognate DCs and rIL-2 (Figure S3D), and CD28-induced phosphorylation of ribosomal protein S6 (Figure S3E). However, rapamycin did not affect CD28-induced migration *in vitro* (Figures S3F and S3G) or *in vivo* (Figures S3H–S3K), suggesting that CD28 promotes Treg cell migration via mediators downstream of PI3K other than mTORC1.

Pro-migratory Stimuli Induce Metabolic Reprogramming

We have previously shown that in Tconv cells, activation of glycolysis during migration occurs via transcriptional and post-transcriptional regulation of the enzyme Hexokinase (HK)I (Haas et al., 2015). We therefore analyzed the expression of a number of glycolytic enzymes by expanded Treg cells 4 hr after CD28 and CTLA-4 stimulation. CD28 stimulation led to a modest increase in HKI, Enolase, and Aldolase expression by Treg cells (Figures 4A and 4B). The most substantial increase was observed in the expression of the HK isoenzyme glucokinase (HKIV or GCK), a rate-limiting enzyme key to hepatocyte and pancreatic beta cell function, whose expression by T cells has not been previously reported. Concomitant CTLA-4 triggering inhibited CD28-induced enzyme expression.

We extended our analysis also to HKII and observed that, like that of GCK, a substantially enhanced expression of this enzyme occurred as early as 5 min after stimulation not only by CD28 signals, but also following LFA-1 triggering by recombinant ICAM-1 (Figures 4C, S4A, and S4B), suggesting that both stimuli enhance enzyme expression also by post-transcriptional mechanisms.

We then measured transcription of the GCK, HKI, and HKII genes, which was indeed increased by LFA-1 or CD28 stimulation (Figures 4D, S4C, and S4D, respectively). As expected, enzyme induction by CD28 was prevented by CTLA-4 triggering. In this set of experiments, transcription of the GCK regulatory protein (GCKR) gene (Figure 4E), a post-transcriptional regulator which blocks free cytoplasmic GCK (Farrelly et al., 1999), was also analyzed. Confocal analysis of expression and co-localization of GCK and GCKR following CD28 and LFA-1 activation confirmed that both CD28 and LFA1 stimuli decrease GCKR expression, concomitant to a substantial increase of GCK availability (Figures 4F and 4G).

To address the relative contribution of HKII and GCK activity to their motility, Treg cells were treated with either the GCK activator AZD1656 (Waring et al., 2012) or with the HKII-selective inhibitor Clotrimazole (CLT), which inhibits the glycolytic flux and respiration in CD3 plus CD28-stimulated Tconv cells (Figures S4E and S4F; van der Windt et al., 2013). GCK activation significantly enhanced Treg cell migration to the inflamed tissue (Figure 4H) but did not affect division (Figure 4I). Conversely, CLT was effective at inhibiting PCNA upregulation by Treg cells (Figure 4J) in response to allogeneic DCs but did not affect rICAM-1-mediated induction of glycolysis (Figure 4K) or migration to inflamed peritoneum *in vivo* (Figure 4L), implying that HKII is redundant for Treg cell migration.

mTORC2-Dependent Induction of GCK Expression Is Required for Treg Cell Migration

The above observations implicate GCK as a key enzyme induced by both CD28- and LFA-1-mediated signals in migrating Treg cells. GCK expression in the liver is regulated by the relatively rapamycin-insensitive mTORC2 (Hagiwara et al., 2012).

Based on this evidence and the observation that CD28-induced Treg cell trafficking is PI3K dependent but rapamycin insensitive (Figures 3 and S3), we examined the contribution of mTORC2 signaling to Treg cell metabolism and migration. First, we confirmed that CD28 triggering led to mTORC2-dependent AKT phosphorylation at the serine residue 473 (Figure 5A). Subsequently, expression of Rictor, an obligatory component of mTORC2, was prevented in expanded Treg cells by lentivirus-delivered, specific shRNAs (Figures S5A and S5B). For comparison we also silenced GCK expression. As a control, cells were transduced with an empty vector (PLKO.1). Gene silencing did not affect cell survival (Figures S5C and S5D). Rictor-depleted Treg cells became unable to upregulate GCK protein expression following CD28 and LFA-1 stimulation

Figure 3. CD28-Induced Migration and Metabolic Reprogramming Require PI3K but Not mTORC-1 Activation

WT and *Cd28*^{Y170F} mice received an i.p. injection of Zymosan. Samples were collected either before or 72 hr after the injection. The presence of Treg cells in the indicated tissues was measured by flow cytometry.

(A) Representative dot plots from 2 independent experiments.

(B) The mean percentage of cells measured in two experiments of identical design ± SD.

(C and D) Ratio of cells retrieved in the indicated tissues over time ± SD (n = 3).

(E) ECAR (±SD) of antibody-stimulated *Cd28*^{Y170F} and WT Treg cells was compared using fluxometry. n = 4, N = 2.

(F) Migration of antibody-stimulated *Cd28*^{Y170F} and WT Treg cells through IFN-γ-treated EC monolayers. Results are expressed as mean percentage of migrated cells after 24 hr ± SD. N = 4.

(G–J) Equal numbers of antibody-stimulated PKH26-labeled WT or *Cd28*^{Y170F} Treg cells were injected i.v. into syngeneic mice treated with IFN-γ i.p. 48 hr earlier. Cells were harvested from the indicated tissues 24 hr later, counter-stained for Foxp3, and analyzed by flow cytometry. Representative dot plots of 2 independent experiments are shown in (G) and (I). The bar graphs in (H) and (J) indicate mean absolute numbers of labeled cells (n = 4, N = 2) ± SD.

*p < 0.05; **p < 0.01; ***p < 0.005. Please see also Figure S3.

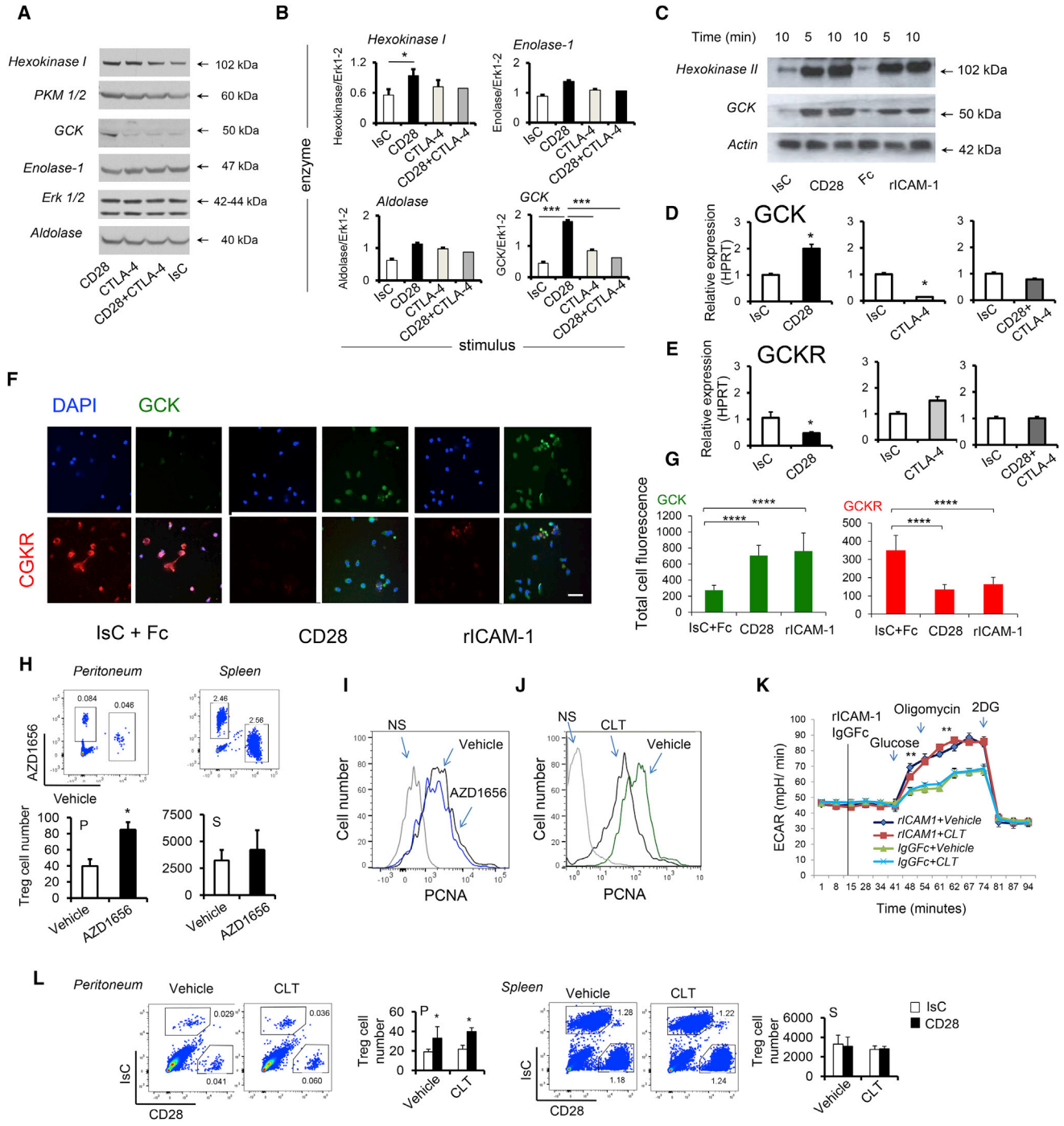

Figure 4. Pro-migratory Stimuli Induce Metabolic Reprogramming of Treg Cells

(A and B) Expression of the indicated enzymes in Treg cells was measured 4 hr after antibody stimulation by western blotting. In (B) the mean relative expression measured by densitometric analysis in 3 independent experiments ± SD is shown.

(C) Expression of the indicated enzymes by CD28- or LFA-1-stimulated Treg cells measured by western blotting at the indicated time points.

(D–G) Relative mRNA expression of GCK (D) and GCKR (E) and cellular protein expression (F and G) by antibody-stimulated Treg cells was measured by RT-PCR and confocal microscopy, respectively. In (G) the mean MFI ± SEM measured using ImageJ software is shown. N = 3. Scale bar 20 μm.

(H) AZD1656 (GCK activator, 1 μM) and vehicle-treated Treg cells (2 hr in insulin-free medium) were labeled with different intravital fluorescent dyes, and co-injected into syngeneic recipients that had received IFN-γ i.p. 48 hr earlier. Cells were recovered from the peritoneum or spleen after 24 hr and analyzed by flow cytometry. Representative dot plots from 2 independent experiments are shown. The bar graphs indicate mean absolute number of labeled cells retrieved ± SD (n = 4, N = 2).

(legend continued on next page)

(Figure 5B), suggesting that this event was mTORC2 dependent. Confocal analysis of Rictor-deficient cells confirmed their failure to upregulate GCK expression in response to the pro-migratory signals compared to mock-transduced cells (Figures 5C and 5D). Furthermore, Treg cells lacking mTORC2 activity did not downregulate GCKR expression (Figure 5E). The ability of Rictor- and GCK-shRNA silenced Treg cells to enhance the glycolytic flux upon CD28 or LFA-1 stimulation was also significantly impaired compared to mock-transduced cells (Figure 5F). A glycolysis stress test showed that, although they were unable to increase the glycolytic flux in response to CD28 and LFA-1 signals, both Rictor- and GCK-deficient Treg cells maintained a basal and maximal glycolytic response (Figures 5G and 5H), while their glycolytic reserve was significantly impaired (Figure 5I).

Despite these metabolic alterations, the suppressive and proliferative capacity of Rictor- and GCK-deficient Treg cells were similar to those of their mock-transduced counterpart (Figures S6A–S6C), indicating that this pathway was not required for these functions.

To assess whether the metabolic impairment resulted in alteration of migratory responses, differentially labeled cells transduced with Rictor- or GCK-specific or control shRNAs underwent CD28 or IsC antibody ligation prior to co-injection in syngeneic recipients, which had received a i.p. injection of IFN-γ 48 hr earlier. Their migration to the peritoneal cavity, spleen, and LN was compared 16 hr later. Both Rictor- and GCK-depleted Treg cell migration to the inflammatory site was severely impaired compared to that by mock-transduced cells and was not enhanced by CD28 activation (Figures 6A and 6B). In addition, although similar numbers of cells were injected, significantly lower numbers of GCK-deficient Treg cells were retrieved in the spleen—where early migration does not require active mechanisms—compared with Rictor-deficient or mock-transduced cells (Figures 6C and 6D). We hypothesized that the severe impairment of GCK-deficient Treg cell cytoskeleton might render them unable to squeeze through the pulmonary capillaries and leave the lungs following injection in the venous blood. Indeed, the ratio of GCK-deficient cells retrieved in the lung and the spleen was significantly increased compared to that of control cells independently of CD28 activation (Figure 6E). In addition, although inefficiently compared to mock-transduced cells, shGCK Treg cells were still capable of migrating through pores with a 5 μm diameter in chemotaxis assays, but failed to migrate through 3 μm pores (Figures 6F and 6G), suggesting a severe impairment of cytoskeletal function as a consequence of loss of GCK activity.

In this context, we observed that pro-migratory activity of CD28 signals was accompanied by intense actin remodeling, which was prevented by CTLA-4 signals (Figures S6D and S6E). Glycolytic enzymes including GCK interact with actin (Clarke and Masters, 1975; Murata et al., 1997) to act as a glycolytic ATP feeder for the ATP-hydrolyzing sodium pump (Na,K-ATPase), thus generating energy required for cytoskeletal rearrangements (Jung et al., 2002). We therefore assessed GCK and Na,K-ATPase localization on the actin cytoskeleton in CD28- and LFA-1-stimulated Treg cells. First, we observed that GCK became associated with actin following CD28 stimulation (Figure S6F). Further, unstimulated cells displayed reduced F-actin and GCK expression, which appeared associated with the cytoskeleton (Figures S6G–S6I). Similarly, ATPase expression was low and only partially co-localized with GCK (Figures S6G, S6H, and S6J). Stimulation of CD28 or ICAM led to intense F-actin formation and upregulation of associated GCK and increased expression of the Na,K-ATPase, which also associated with GCK (Figures S6G–S6I). As expected, since shRictor-silenced Treg cells produce less GCK, the amount of co-localization with F-actin was also lower.

To further confirm the selective impact of Rictor and GCK deficiency on Treg cell motility, we finally compared the ability of adoptively transferred (10^7/mouse) control, Rictor-deficient, or GCK-deficient cells to delay rejection of fully allogeneic skin grafts. As expected, Rictor- and GCK-depleted Treg cells failed to prolong graft survival (Figure 6H) as they did not localize in the graft (Figures 6I and 6J) compared to mock-transduced cells. In line with previous results, fewer GCK-deficient cells were found also in the spleen.

Human Treg Cells from Homozygous Carriers of a Loss-of-Function Polymorphism in the GCKR Gene Display Enhanced Motility

To test the physiological relevance of this pathway in the human system, we analyzed the number and functional behavior of circulating Treg cells (defined as $CD25^{hi}CD127^{lo}$) from carriers of a loss-of-function polymorphism in the GCKR gene (C to T, P446L). P446L-GCKR has reduced inhibitory activity toward GCK and has been associated with decreased fasting plasma glucose and enhanced triglyceride synthesis (these parameters measured in our study population are shown in Figures S7A and S7B) via increased GCK activity in the liver of homozygous carriers (Beer et al., 2009).

The number of circulating Treg cells was decreased in carriers of the rare allele 446L of GCKR gene compared to carriers of the WT allele (Figures 7A, 7B, S7A, and S7B) while other $CD4^+$ T cell populations were unaffected (Figures 7C–7E). Importantly, 446L-GCKR Treg cells displayed increased chemokine-induced motility compared to WT-GCKR Treg cells, while Tconv cell

(I and J) expression of PCNA by Treg cells stimulated with allogeneic DCs following treatment with either AZD1656 (I) or Clotrimazole (CLT, 1 μM, 2 hours, J) or vehicle alone was measured by flow cytometry. NS, non-stimulated control cells. Representative histograms from 3 independent experiments are shown. (n = 3, N = 3).

(K) ECAR of Treg cells activated with recombinant ICAM-1 or Fc control. CLT or vehicle as well as other glycolysis-affecting drugs were added as indicated.

(L) CLT- or vehicle-treated Treg cells underwent CD28 or isotype-matched antibody stimulation, labeled with different intravital fluorescent dyes, and injected i.v. in syngeneic recipients that had received IFN-γ i.p. 48 hr earlier. Cells were recovered from the peritoneum (P) or spleen (S) after 24 hr and analyzed by flow cytometry. Representative dot plots from 2 independent experiments are shown. The column graphs indicate mean absolute number of labeled cells retrieved ± SD (n = 3, N = 2).

*p < 0.05 ***p < 0.005; ****p < 0.001. Please see also Figure S4.

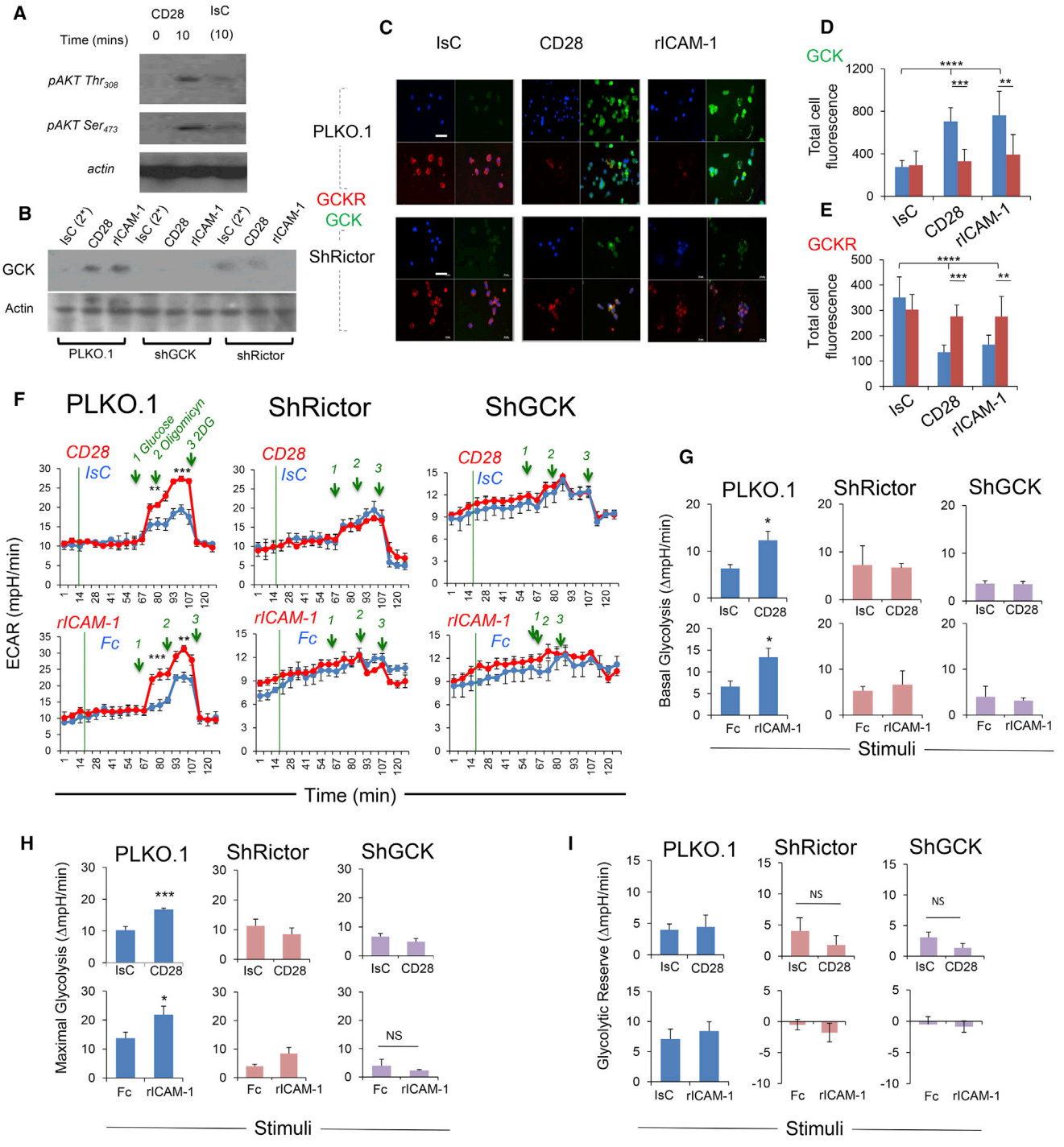

Figure 5. mTORC2 Controls Metabolic Reprogramming Induced by Pro-migratory Stimuli

(A) Phosphorylation of AKT at Thr_{308} and Ser_{473} in Treg cells activated with CD28- or IsC-antibody ligation was measured by immunoblotting.

(B) Treg cells were virally transfected with Rictor-specific or GCK-specific or non-sense (PLKO.1) sh-RNAs, as described in STAR Methods. Expression of GCK was measured by immunoblotting 24 hr later.

(C–E) Expression of GCK and GCKR by control or Rictor-deficient Treg cells following CD28 or LFA-1 activation for 45 min. Bar graphs (D and E) show the mean protein expression (Total cell fluorescence) measured in 3 independent experiments by ImageJ software ± SD. Scale bar, 40 μm.

(F–I) ECAR of CD28- or LFA-1-stimulated Rictor- and GCK-deficient and control T cells was measured with an extracellular flux analyzer. A glycolysis stress assay was performed by adding the indicated compounds at the time points indicated by the green lines. The basal and maximal glycolysis and the glycolytic reserve are shown in (G), (H), and (I), respectively (±SEM). N = 2.

*p < 0.05 ***p < 0.005; ****p < 0.001. Please see also Figure S5.

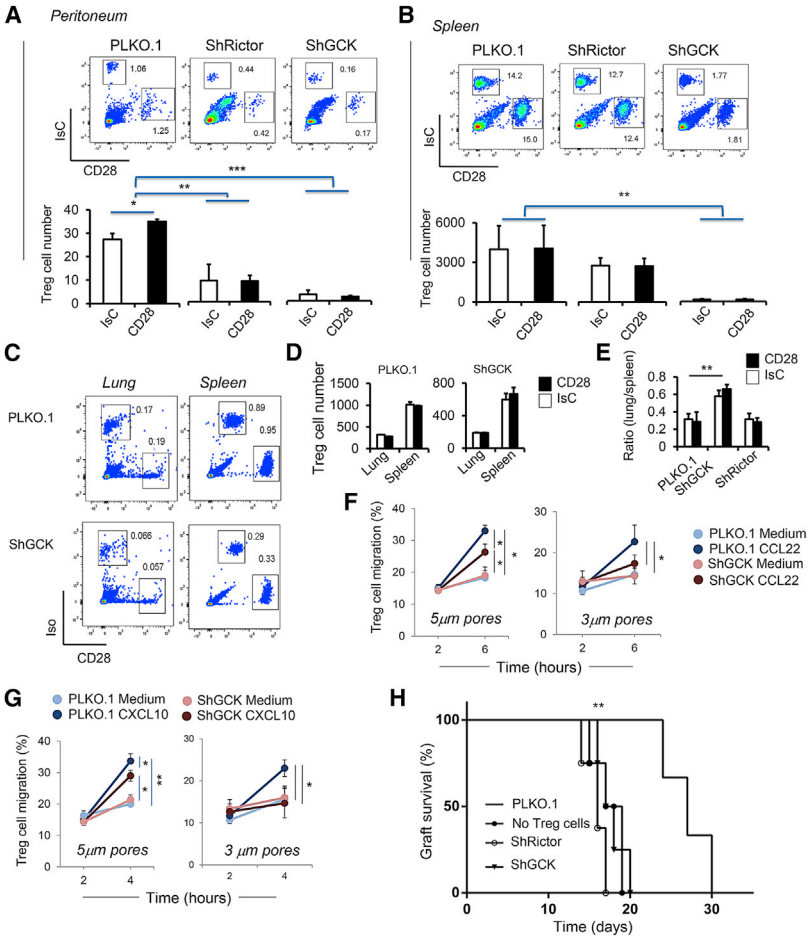

Figure 6. Rictor-Deficient Treg Cells Display Impaired Motility

(A–E) CD28-stimulated or IsC-treated PLKO.1, Rictor- or GCK-deficient Treg cells were labeled with PKH26 and co-injected i.v. with identical numbers of IsC-treated CFSE-labeled cells in syngeneic recipients treated with IFN-γ 48 hr earlier. The presence of differently labeled cells in the indicated organs was assessed by flow cytometry 24 hr later. Representative dot plots from 3 independent experiments are shown on top in (A), (B), and (C). The bar graphs in (A), (B), and (D) indicate mean absolute number of labeled Treg cells recovered in the indicated tissues from 4 different recipients ± SD (N = 3). The bar graph in (E) shows the ratio of Treg cells recovered in the lung and the spleen (n = 4) ± SD.

(F and K) Control and ShGCK Treg cell migration through 5 or 3 μm pore bare-filter transwells in response to CCL22 (F) or CXCL10 (K). Results are expressed as percentage of migrated cells at the indicated time points ± SD (n = 3).

(H–J) BALB/c-derived skin was grafted onto C57BL/6 recipients who had received mock-transduced, Rictor- or GCK-depleted Treg cells or no cells 24 hr earlier. Graft rejection was monitored daily (H). Some grafts were removed 5 days post-grafting and the presence of fluorescently labeled Treg cells in the indicated tissue was assessed by widefield fluorescence microscopy. Representative images of grafts and spleens from 2 independent experiments are shown in (I). The bar graphs (J) indicate the mean number of labeled cells detected in at least 10 10× tissue images from each animal ± SD (n = 8).

*p < 0.05 **p < 0.01; ***p < 0.005. Please see also Figure S6.

migration was unaffected (Figures 7F and 7G). The suppressive ability and phenotype of P446L-GCKR Treg cells did not significantly differ from that of WT-GCKR Treg cells (Figures S7C–S7H), including expression of CCR7 (Figures 7H and 7I), the receptor for the chemokines used in the migration assays. In addition, chemokine-induced molecular events upstream of GCK activation, including glucose uptake (Figures S7I–S7L) and AKT phosphorylation at serine 473 (Figures S7M–S7P), were comparable in 446L- and 446P (WT)-GCKR Treg and Tconv cells, in further support of a key role of increased GCK availability in enhanced 446L-GCKR Treg cell motility.

Collectively these observations suggest that GCK contributes to human Treg cell migration.

DISCUSSION

In this study we have investigated the metabolic pathways that sustain migration of thymic Treg cells and how these pathways become engaged by pro-migratory signals.

Our data indicate that migratory stimuli induce metabolic reprogramming of Treg cells toward aerobic glycolysis. However, while induction of the glycolytic pathway in dividing Treg lymphocytes relies upon mTORC1 activity (Gerriets et al., 2016; Procaccini et al., 2010), activation of glucose metabolism induced by pro-migratory stimuli occurs via mTORC2.

The molecular mechanism for the selective engagement of mTORC2 for the induction of motility-associated glycolysis in Treg cells remains unclear. Physiologically, Treg cells display high activity of rapamycin-sensitive mTOR phosphorylation, which is transiently inhibited by environmental stimuli to allow their proliferation *in vivo* (Procaccini et al., 2010). A simplistic explanation is that constitutively high mTORC1 activation might limit its availability for additional signals. Thus, glycolysis-activating stimuli in non-proliferating Treg cells may be redirected to the mTORC2 pathway.

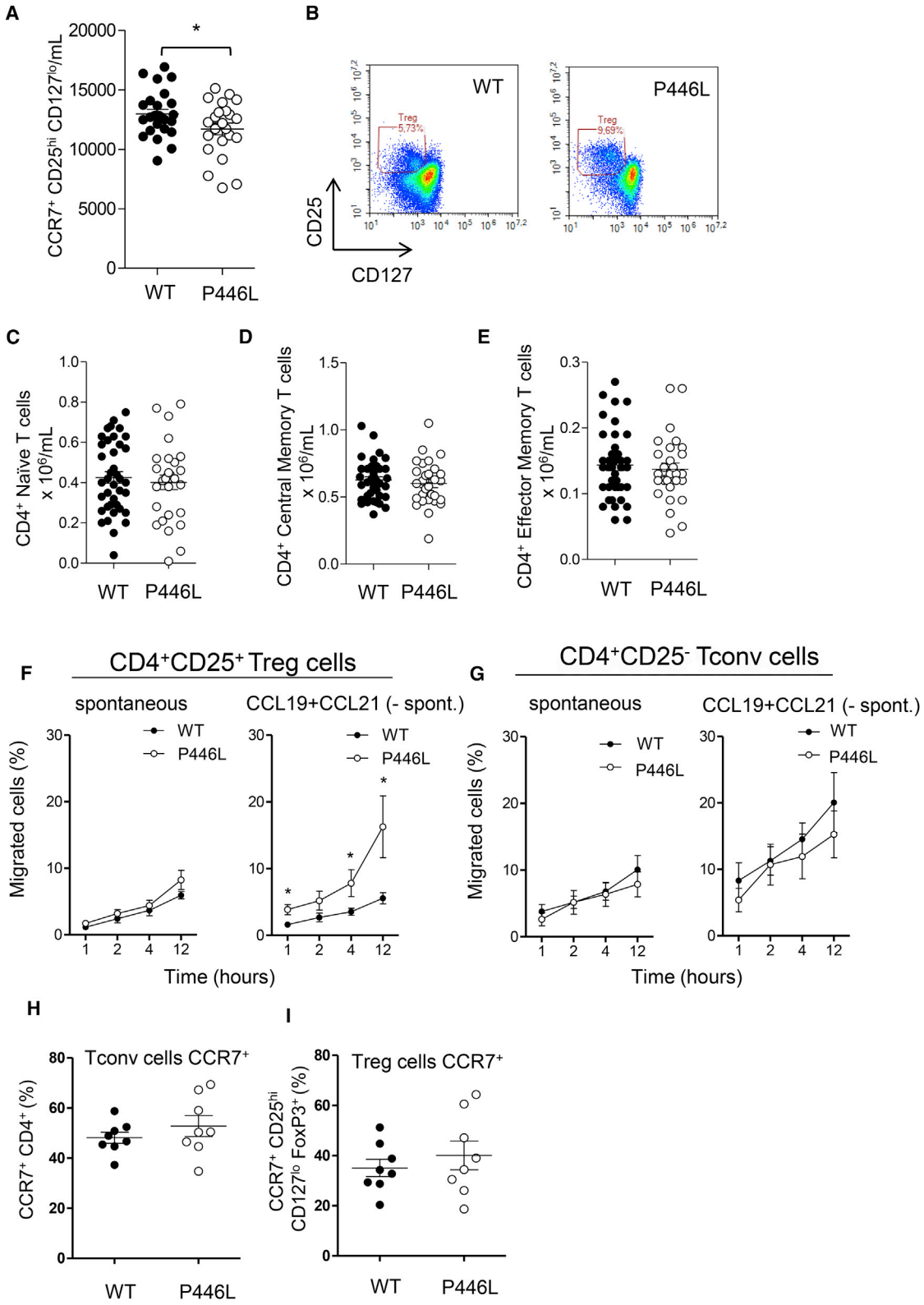

Figure 7. Treg Cells Bearing a Loss-of-Function GCKR Allele Display Enhanced Motility

(A) Cell number/mL of Treg cells ($CD4^+CD25^{hi}CD127^{lo}$) in carriers of the allele P446L compared to individuals carrying the WT allele (P446).

(B) Dot plots representative of 25 individuals analyzed.

(legend continued on next page)

Consistent with this hypothesis, mTORC2 regulates the glycolytic flux by fully activating AKT and controlling c-Myc expression which in turn regulate the transcription of genes that control glucose transport and glycolysis, including GLUT1 and HKII (Masui et al., 2014). Finally, mTORC2 is known to mediate cytoskeleton reorganization (Cybulski and Hall, 2009) and substantial evidence suggests that its activation requires PI3K activity (Boulbes et al., 2010; Gan et al., 2011), but its ability to promote cell migration via modulation of metabolic pathways has not previously been described.

The dichotomy between regulation of glycolysis during Treg cell proliferation and migration is also reflected in the enzymatic machinery engaged for these cellular responses. Metabolic reprogramming following antigen activation of conventional T cell involves a substantial increase of hexokinase activity, which is dependent on a transcriptional switch in HK isozyme expression from HKI to HKII, which has higher affinity for glucose (Bosca et al., 1988; Marjanovic et al., 1990; Wang et al., 2011). In addition—and as a likely consequence of mTORC2 activation—pro-migratory signals substantially enhance GCK expression. In line with the non-redundant role of mTORC2 in the metabolic regulation of motility, GKC has been shown to be one of the main targets downstream of mTORC2-mediated signaling in the liver (Hagiwara et al., 2012).

We have also provided evidence that this pathway might be operational in the human immune system. The number of circulating Treg cells was decreased in carriers of a GCKR loss-of-function variant and mutant Treg cells display enhanced motility, suggesting increased localization in tissues. Importantly, migration of Tconv cells is not affected by loss of GCKR inhibition and increased GCK activity. The impact of enhanced Treg cell trafficking on immune responses in these individuals will require further investigation.

The physiological significance of preferential utilization of GCK by migrating Treg cells remains to be defined by the use of mice with T cell-specific GCK deficiency. Unlike other hexokinases, GCK has a much lower affinity for glucose, which is within the physiological plasma glucose range (S0.5 ≈7 mM) and is less susceptible to inhibition by the glycolysis metabolite glucose 6-phosphate (Lenzen, 2014). The use of GCK by Treg cells might explain the previous report of a delayed polarization rate of Treg cells, compared to Tconv cells, in response to CD28 stimulation (Müller et al., 2008). CD28-stimulated Treg cells undergo early and late waves of migration, which might reflect the posttranscriptional and transcriptional increase in GCK expression, which we observed. GCK—which is not inhibited by glycolysis metabolites—might also maintain the glycolytic flux and survival in chronic inflammatory sites rich of inhibitory glycolysis metabolites, giving Treg cells an advantage over Tconv cells. In such environments, Tconv cells tend to become hyporesponsive and lose their function as a consequence, for example, of exposure to lactate (Haas et al., 2015). Alternatively, or in addition, dependency on low-affinity GCK might promote retention of Treg cells in glucose-depleted tissues such as tumors.

During immune responses, the ability of CD28 and CTLA-4 to function as a metabolic switch might at least in part explain their opposing effects on T cell division and function. For example, transient CTLA-4 expression following activation might serve to shut down glycolysis, thus supporting reprogramming of long-lived memory $CD8^+$ T cells to FAO (O'Sullivan et al., 2014), thus promoting the contraction phase of T cell responses and maintaining homeostasis by favoring the induction of anergy (Zheng et al., 2009).

While the functional effects of CTLA-4 in the regulation of effector immunity are well established, the contribution of CTLA-4 to Treg cell function is not completely understood. CTLA-4-deficient mice display normal numbers of Treg lymphocytes, which however appear to be defective in their suppressive function *in vivo* (Wing et al., 2008) but not *in vitro* (Tang et al., 2004). Our observations suggest that, by antagonizing CD28-induced migratory signals, CTLA-4 might be required for tissue retention rather than for Treg cell suppressive activity.

Impaired migration of $Cd28^{Y170F}$ Treg cells in response to activation of innate immunity also indicates that CD28 signals instruct their mobilization and redistribution from lymphoid tissue – where CD28 engagement is likely to take place during interaction with activated DCs - to the blood stream. CD28-induced pro-migratory signals might dominate in the absence of cognate interactions thus supporting Treg cell recirculation. In contrast, transient upregulation of CTLA-4 by antigen-activation may reduce their motility leading to retention within tissues.

In summary, this study defines a pathway for the metabolic regulation of motility and migration induced in Treg cells by pro-migratory stimuli. The apparent selectivity of this pathway in the regulation of motility of both murine and human Treg cells suggest that it might be possible to selectively manipulate trafficking of distinct lymphocyte subsets by targeting different glycolytic enzymes. Further, as the signaling mediators involved in the metabolic reprogramming of proliferating Treg cells are distinct from those regulating motility, selective targeting of these enzymes might allow the modulation of distinct functions in therapeutic settings.

STAR★METHODS

Detailed methods are provided in the online version of this paper and include the following:

- KEY RESOURCES TABLE
- CONTACT FOR REAGENT AND RESOURCE SHARING
- EXPERIMENTAL MODEL AND SUBJECT DETAILS

(C–E) $CD4^+$ lymphocyte subpopulations, defined as naive ($CD45RA^+$), central memory ($CD45RO^+CD62L^+CCR7^+$), and effector memory ($CD45RO^+CD62L^-CCR7^-$) in the two study populations.

(F and G) Migratory responses of Treg (F) and Tconv (G) cells from eight P446L-GCKR carriers or WT-GCKR individuals to the chemokines CCL19 and CCL21 were measured by bare-filter 5 μm diameter transwells.

(H and I) The percentage of T cells expressing CCR7, receptor for the chemokines CCL19 and CCL 21 used in the migration assays, from P446L-GCKR carriers (n = 8) and WT-GCKR (n = 8) subjects are shown.

*$p < 0.05$. Please see also Figure S7.

SUPPLEMENTAL INFORMATION

Supplemental Information includes seven figures and can be found with this article online at https://doi.org/10.1016/j.immuni.2017.10.017.

AUTHORS CONTRIBUTIONS

Conceptualization, F.M.M.-B., G.M., C.M., D.M.S., V.D.R., and G.D.N.; Investigation and Formal Analysis, M.K., K.C.P.C., H.F., F.B., G.W., D.C., E.J.W., A.C., M.J., and R.H.; Writing – Original Draft, Visualization, M.K., K.C.P.C., M.J., G.D.N., and F.M.M.-B.; Writing – Review & Editing, F.M.M.-B., C.M., G.M., V.D.R., and G.D.N.; Funding Acquisition, Project Administration, F.M.M.-B.; Resources, A.B., D.M.S., K.O., D.C.W., and A.L.C.; Supervision, F.M.M.-B., V.D.R., and G.D.N.

ACKNOWLEDGMENTS

We thank Fulvio D'Acquisto for helpful discussions. F.M.M.-B. is supported by the British Heart Foundation grants CH/15/2/32064 and RG/14/2/30616 and by the Barts Charity grant MGU0377, G.M. is supported by the Fondazione Italiana Sclerosi Multipla (grant no. 2016/R/18), V.D.R. is supported by the Associazione Italiana per la Ricerca sul Cancro-Cariplo Transforming IDEas in Oncological Research (TRIDEO) (grant no. 17447), and G.D.N. is supported by Fondazione Cariplo 2016-0852 and Ministero della Salute GR-2011-02346974. D.M.S. is employed by and holds shares in AstraZeneca Plc.

Received: December 22, 2016
Revised: June 30, 2017
Accepted: October 26, 2017
Published: November 21, 2017

REFERENCES

Baragetti, A., Palmen, J., Garlaschelli, K., Grigore, L., Pellegatta, F., Tragni, E., Catapano, A.L., Humphries, S.E., Norata, G.D., and Talmud, P.J. (2015). Telomere shortening over 6 years is associated with increased subclinical carotid vascular damage and worse cardiovascular prognosis in the general population. J. Intern. Med. *277*, 478–487.

Beer, N.L., Tribble, N.D., McCulloch, L.J., Roos, C., Johnson, P.R., Orho-Melander, M., and Gloyn, A.L. (2009). The P446L variant in GCKR associated with fasting plasma glucose and triglyceride levels exerts its effect through increased glucokinase activity in liver. Hum. Mol. Genet. *18*, 4081–4088.

Bernstein, B.W., and Bamburg, J.R. (2003). Actin-ATP hydrolysis is a major energy drain for neurons. J. Neurosci. *23*, 1–6.

Bosca, L., Mojena, M., Diaz-Guerra, J.M., and Marquez, C. (1988). Phorbol 12,13-dibutyrate and mitogens increase fructose 2,6-bisphosphate in lymphocytes. Comparison of lymphocyte and rat-liver 6-phosphofructo-2-kinase. Eur. J. Biochem. *175*, 317–323.

Boulbes, D., Chen, C.H., Shaikenov, T., Agarwal, N.K., Peterson, T.R., Addona, T.A., Keshishian, H., Carr, S.A., Magnuson, M.A., Sabatini, D.M., and Sarbassov, D. (2010). Rictor phosphorylation on the Thr-1135 site does not require mammalian target of rapamycin complex 2. Mol. Cancer Res. *8*, 896–906.

Chang, T.T., Jabs, C., Sobel, R.A., Kuchroo, V.K., and Sharpe, A.H. (1999). Studies in B7-deficient mice reveal a critical role for B7 costimulation in both induction and effector phases of experimental autoimmune encephalomyelitis. J. Exp. Med. *190*, 733–740.

Chi, H. (2012). Regulation and function of mTOR signalling in T cell fate decisions. Nat. Rev. Immunol. *12*, 325–338.

Clarke, F.M., and Masters, C.J. (1975). On the association of glycolytic enzymes with structural proteins of skeletal muscle. Biochim. Biophys. Acta *381*, 37–46.

Cybulski, N., and Hall, M.N. (2009). TOR complex 2: a signaling pathway of its own. Trends Biochem. Sci. *34*, 620–627.

Dang, E.V., Barbi, J., Yang, H.Y., Jinasena, D., Yu, H., Zheng, Y., Bordman, Z., Fu, J., Kim, Y., Yen, H.R., et al. (2011). Control of T(H)17/T(reg) balance by hypoxia-inducible factor 1. Cell *146*, 772–784.

Farrelly, D., Brown, K.S., Tieman, A., Ren, J., Lira, S.A., Hagan, D., Gregg, R., Mookhtiar, K.A., and Hariharan, N. (1999). Mice mutant for glucokinase regulatory protein exhibit decreased liver glucokinase: a sequestration mechanism in metabolic regulation. Proc. Natl. Acad. Sci. USA *96*, 14511–14516.

Frauwirth, K.A., Riley, J.L., Harris, M.H., Parry, R.V., Rathmell, J.C., Plas, D.R., Elstrom, R.L., June, C.H., and Thompson, C.B. (2002). The CD28 signaling pathway regulates glucose metabolism. Immunity *16*, 769–777.

Fu, H., Kishore, M., Gittens, B., Wang, G., Coe, D., Komarowska, I., Infante, E., Ridley, A.J., Cooper, D., Perretti, M., and Marelli-Berg, F.M. (2014). Self-recognition of the endothelium enables regulatory T-cell trafficking and defines the kinetics of immune regulation. Nat. Commun. *5*, 3436.

Gan, X., Wang, J., Su, B., and Wu, D. (2011). Evidence for direct activation of mTORC2 kinase activity by phosphatidylinositol 3,4,5-trisphosphate. J. Biol. Chem. *286*, 10998–11002.

Gerriets, V.A., Kishton, R.J., Johnson, M.O., Cohen, S., Siska, P.J., Nichols, A.G., Warmoes, M.O., de Cubas, A.A., MacIver, N.J., Locasale, J.W., et al. (2016). Foxp3 and Toll-like receptor signaling balance Treg cell anabolic metabolism for suppression. Nat. Immunol. *17*, 1459–1466.

Haas, R., Smith, J., Rocher-Ros, V., Nadkarni, S., Montero-Melendez, T., D'Acquisto, F., Bland, E.J., Bombardieri, M., Pitzalis, C., Perretti, M., et al.

(2015). Lactate regulates metabolic and pro-inflammatory circuits in control of T cell migration and effector functions. PLoS Biol. *13*, e1002202.

Hagiwara, A., Cornu, M., Cybulski, N., Polak, P., Betz, C., Trapani, F., Terracciano, L., Heim, M.H., Rüegg, M.A., and Hall, M.N. (2012). Hepatic mTORC2 activates glycolysis and lipogenesis through Akt, glucokinase, and SREBP1c. Cell Metab. *15*, 725–738.

Jacobs, S.R., Herman, C.E., Maciver, N.J., Wofford, J.A., Wieman, H.L., Hammen, J.J., and Rathmell, J.C. (2008). Glucose uptake is limiting in T cell activation and requires CD28-mediated Akt-dependent and independent pathways. J. Immunol. *180*, 4476–4486.

Jain, N., Miu, B., Jiang, J.K., McKinstry, K.K., Prince, A., Swain, S.L., Greiner, D.L., Thomas, C.J., Sanderson, M.J., Berg, L.J., and Kang, J. (2013). CD28 and ITK signals regulate autoreactive T cell trafficking. Nat. Med. *19*, 1632–1637.

Jarmin, S.J., David, R., Ma, L., Chai, J.-G., Dewchand, H., Takesono, A., Ridley, A.J., Okkenhaug, K., and Marelli-Berg, F.M. (2008). T cell receptor-induced phosphoinositide-3-kinase p110delta activity is required for T cell localization to antigenic tissue in mice. J. Clin. Invest. *118*, 1154–1164.

Jung, J., Yoon, T., Choi, E.C., and Lee, K. (2002). Interaction of cofilin with triose-phosphate isomerase contributes glycolytic fuel for Na,K-ATPase via Rho-mediated signaling pathway. J. Biol. Chem. *277*, 48931–48937.

Lenzen, S. (2014). A fresh view of glycolysis and glucokinase regulation: history and current status. J. Biol. Chem. *289*, 12189–12194.

Livak, K.J., and Schmittgen, T.D. (2001). Analysis of relative gene expression data using real-time quantitative PCR and the 2(-Delta Delta C(T)) Method. Methods *25*, 402–408.

Lorenz, M.W., Polak, J.F., Kavousi, M., Mathiesen, E.B., Völzke, H., Tuomainen, T.P., Sander, D., Plichart, M., Catapano, A.L., Robertson, C.M., et al.; PROG-IMT Study Group (2012). Carotid intima-media thickness progression to predict cardiovascular events in the general population (the PROG-IMT collaborative project): a meta-analysis of individual participant data. Lancet *379*, 2053–2062.

Marelli-Berg, F.M., Peek, E., Lidington, E.A., Stauss, H.J., and Lechler, R.I. (2000). Isolation of endothelial cells from murine tissue. J. Immunol. Methods *244*, 205–215.

Marjanovic, S., Eriksson, I., and Nelson, B.D. (1990). Expression of a new set of glycolytic isozymes in activated human peripheral lymphocytes. Biochim. Biophys. Acta *1087*, 1–6.

Masui, K., Cavenee, W.K., and Mischel, P.S. (2014). mTORC2 in the center of cancer metabolic reprogramming. Trends Endocrinol. Metab. *25*, 364–373.

Michalek, R.D., Gerriets, V.A., Jacobs, S.R., Macintyre, A.N., MacIver, N.J., Mason, E.F., Sullivan, S.A., Nichols, A.G., and Rathmell, J.C. (2011). Cutting edge: distinct glycolytic and lipid oxidative metabolic programs are essential for effector and regulatory CD4+ T cell subsets. J. Immunol. *186*, 3299–3303.

Mirenda, V., Jarmin, S.J., David, R., Dyson, J., Scott, D., Gu, Y., Lechler, R.I., Okkenhaug, K., and Marelli-Berg, F.M. (2007). Physiologic and aberrant regulation of memory T-cell trafficking by the costimulatory molecule CD28. Blood *109*, 2968–2977.

Müller, N., van den Brandt, J., Odoardi, F., Tischner, D., Herath, J., Flügel, A., and Reichardt, H.M. (2008). A CD28 superagonistic antibody elicits 2 functionally distinct waves of T cell activation in rats. J. Clin. Invest. *118*, 1405–1416.

Murata, T., Katagiri, H., Ishihara, H., Shibasaki, Y., Asano, T., Toyoda, Y., Pekiner, B., Pekiner, C., Miwa, I., and Oka, Y. (1997). Co-localization of glucokinase with actin filaments. FEBS Lett. *406*, 109–113.

Newson, J., Stables, M., Karra, E., Arce-Vargas, F., Quezada, S., Motwani, M., Mack, M., Yona, S., Audzevich, T., and Gilroy, D.W. (2014). Resolution of acute inflammation bridges the gap between innate and adaptive immunity. Blood *124*, 1748–1764.

Norata, G.D., Garlaschelli, K., Ongari, M., Raselli, S., Grigore, L., and Catapano, A.L. (2006). Effects of fractalkine receptor variants on common carotid artery intima-media thickness. Stroke *37*, 1558–1561.

Norata, G.D., Garlaschelli, K., Grigore, L., Tibolla, G., Raselli, S., Redaelli, L., Buccianti, G., and Catapano, A.L. (2009). Circulating soluble receptor for advanced glycation end products is inversely associated with body mass index and waist/hip ratio in the general population. Nutr. Metab. Cardiovasc. Dis. *19*, 129–134.

O'Sullivan, D., van der Windt, G.J., Huang, S.C., Curtis, J.D., Chang, C.H., Buck, M.D., Qiu, J., Smith, A.M., Lam, W.Y., DiPlato, L.M., et al. (2014). Memory CD8(+) T cells use cell-intrinsic lipolysis to support the metabolic programming necessary for development. Immunity *41*, 75–88.

Okkenhaug, K., Wu, L., Garza, K.M., La Rose, J., Khoo, W., Odermatt, B., Mak, T.W., Ohashi, P.S., and Rottapel, R. (2001). A point mutation in CD28 distinguishes proliferative signals from survival signals. Nat. Immunol. *2*, 325–332.

Parry, R.V., Chemnitz, J.M., Frauwirth, K.A., Lanfranco, A.R., Braunstein, I., Kobayashi, S.V., Linsley, P.S., Thompson, C.B., and Riley, J.L. (2005). CTLA-4 and PD-1 receptors inhibit T-cell activation by distinct mechanisms. Mol. Cell. Biol. *25*, 9543–9553.

Powell, J.D., and Delgoffe, G.M. (2010). The mammalian target of rapamycin: linking T cell differentiation, function, and metabolism. Immunity *33*, 301–311.

Procaccini, C., De Rosa, V., Galgani, M., Abanni, L., Calì, G., Porcellini, A., Carbone, F., Fontana, S., Horvath, T.L., La Cava, A., and Matarese, G. (2010). An oscillatory switch in mTOR kinase activity sets regulatory T cell responsiveness. Immunity *33*, 929–941.

Schneider, H., Valk, E., da Rocha Dias, S., Wei, B., and Rudd, C.E. (2005). CTLA-4 up-regulation of lymphocyte function-associated antigen 1 adhesion and clustering as an alternate basis for coreceptor function. Proc. Natl. Acad. Sci. USA *102*, 12861–12866.

Shi, L.Z., Wang, R., Huang, G., Vogel, P., Neale, G., Green, D.R., and Chi, H. (2011). HIF1alpha-dependent glycolytic pathway orchestrates a metabolic checkpoint for the differentiation of TH17 and Treg cells. J. Exp. Med. *208*, 1367–1376.

Tai, X., Cowan, M., Feigenbaum, L., and Singer, A. (2005). CD28 costimulation of developing thymocytes induces Foxp3 expression and regulatory T cell differentiation independently of interleukin 2. Nat. Immunol. *6*, 152–162.

Tang, Q., Boden, E.K., Henriksen, K.J., Bour-Jordan, H., Bi, M., and Bluestone, J.A. (2004). Distinct roles of CTLA-4 and TGF-beta in CD4+CD25+ regulatory T cell function. Eur. J. Immunol. *34*, 2996–3005.

Tang, Q., Bluestone, J.A., and Kang, S.M. (2012). CD4(+)Foxp3(+) regulatory T cell therapy in transplantation. J. Mol. Cell Biol. *4*, 11–21.

van der Windt, G.J., O'Sullivan, D., Everts, B., Huang, S.C., Buck, M.D., Curtis, J.D., Chang, C.H., Smith, A.M., Ai, T., Faubert, B., et al. (2013). CD8 memory T cells have a bioenergetic advantage that underlies their rapid recall ability. Proc. Natl. Acad. Sci. USA *110*, 14336–14341.

Wang, R., Dillon, C.P., Shi, L.Z., Milasta, S., Carter, R., Finkelstein, D., McCormick, L.L., Fitzgerald, P., Chi, H., Munger, J., and Green, D.R. (2011). The transcription factor Myc controls metabolic reprogramming upon T lymphocyte activation. Immunity *35*, 871–882.

Waring, M.J., Clarke, D.S., Fenwick, M.D., Godfrey, L., Groombridge, S.D., Johnstone, C., McKerrecher, D., Pike, K.G., Rayner, J.W., Robb, G.R., and Wilson, I. (2012). Property based optimisation of glucokinase activators - discovery of the phase IIb clinical candidate AZD1656. MedChemComm *3*, 1077–1081.

Wells, A.D., Walsh, M.C., Bluestone, J.A., and Turka, L.A. (2001). Signaling through CD28 and CTLA-4 controls two distinct forms of T cell anergy. J. Clin. Invest. *108*, 895–903.

Wieman, H.L., Wofford, J.A., and Rathmell, J.C. (2007). Cytokine stimulation promotes glucose uptake via phosphatidylinositol-3 kinase/Akt regulation of Glut1 activity and trafficking. Mol. Biol. Cell *18*, 1437–1446.

Wing, K., Onishi, Y., Prieto-Martin, P., Yamaguchi, T., Miyara, M., Fehervari, Z., Nomura, T., and Sakaguchi, S. (2008). CTLA-4 control over Foxp3+ regulatory T cell function. Science *322*, 271–275.

Zheng, Y., Delgoffe, G.M., Meyer, C.F., Chan, W., and Powell, J.D. (2009). Anergic T cells are metabolically anergic. J. Immunol. *183*, 6095–6101.

STAR★METHODS

KEY RESOURCES TABLE

REAGENT or RESOURCE	SOURCE	IDENTIFIER
Antibodies		
Mouse Anti-CD3-PECY7	Biolegend	100220; RRID: AB_1732057
Mouse Anti-CD4-PE	eBioscience	12-0042-82; RRID: AB_465510
Mouse Anti-Foxp3-APC	eBioscience	77-5775-40; RRID: AB_4699981
Mouse Anti-CD8-APC	eBioscience	11-0081-82; RRID: AB_464915
Mouse Anti-CD11a-PE-FITC	eBioscience	11-0111-81; RRID: AB_464930
Mouse Anti-CD11c-AF647	Biolegend	117312; RRID: AB_389328
Mouse Anti-CD14-PE	eBioscience	12-0141-82; RRID: AB_465563
Mouse Anti-CD25-PECY7	eBioscience	12-0251-81; RRID: AB_465606
Mouse Anti-CD28-PE	eBioscience	12-0281-82; RRID: AB_465621
Phospho-Akt1 (Ser473)- APC	eBioscience	Cat # 17-9715-41; RRID: AB_2573309
Mouse Anti-CD29-APC/CY7	Biolegend	102226; RRID: AB_2128076
Mouse Anti-CD31-PE	eBioscience	12-0311-81; RRID: AB_465631
Mouse Anti-CD40-PE-FITC	Biolegend	124607; RRID: AB_1134090
Mouse Anti-CD49d-PE	Biolegend	103705; RRID: AB_313046
Mouse Anti-CD54-PE-FITC	Biolegend	116105; RRID: AB_313696
Mouse Anti-Glut1-PE	Novusbio	NB110-39113PE
Mouse Anti-CD62L-FITC	Biolegend	104405; RRID: AB_313092
Mouse Anti- CCR4-APC	Biolegend	131211; RRID: AB_1279135
Mouse Anti-CCR7-APC	Biolegend	120107; RRID: AB_389233
Anti- LPAM-1-APC	Biolegend,	120607; RRID: AB_10719833
anti-hexokinase-1- C35C4	Cell signaling	Cat.# 2024
anti-CPT1A-D3B3	Cell signaling	Cat.# 12252
anti-enolase-1	Cell signaling	Cat.# 3810; RRID: AB_2246524
anti-aldolase A	Cell signaling	Cat.# 3188; RRID: AB_2226674
p-S6 (Ser240 and Ser244)	Cell signaling	Cat.# 2215; RRID: AB_331683
anti-S6-5G10	Cell signaling	Cat.# 2217; RRID: AB_331355
Phospho-Akt (Ser473) Antibody	Cell signaling	#9271; RRID: AB_329825
Akt (pan) (C67E7) Rabbit mAb	Cell signaling	#4691; RRID: AB_915783
anti-GCK -H88	Santa Cruz Biotechnology	Cat.# SC7908; RRID: AB_2107620
anti-actin-I19	Santa Cruz Biotechnology	Cat.# SC1616; RRID: AB_630836
anti-Erk1/2 (H72)	Santa Cruz Biotechnology	Cat.# SC292838; RRID: AB_2650548
rat anti-mouse CD8 depletion antibody, clone 53-6.7	eBioscience	14-0081-82; RRID: AB_467087
anti-mouse CD3	eBiosciences	Cat# 16-0032-85; RRID: AB_468852
anti-mouse CD28	eBiosciences	Cat# 16-0281-86; RRID: AB_468923
hamster anti-mouse CD28 (clone: 37.52),	Bio-Rad	Cat# MCA1363; RRID: AB_321560
goat anti-hamster immunoglobulin (Ig)	Bio-Rad	Cat# STAR104; RRID: AB_323008
anti-mouse CTLA-4 (clone: UC10-4F10-11)	Becton Dickinson	Cat# 553718
hamster IgG isotype control	Bio-Rad	Cat# MCA2356; RRID: AB_567313
Human IgG Fc fragment	Merck Millipore	AG714; RRID: AB_97863
DAPI (4',6-diamidino-2-phenylindole)	LifeTechnologies	Cat# D1306; RRID: AB_2629482
alpha 1 Na,K-ATPase antibody [M8-PI-A3]	Abcam	ab2872; RRID: AB_2061140
Rabbit Anti-mouse Rictor	Abcam	ab70374; RRID: AB_2253794
Anti-Glucokinase	Abcam	ab88056; RRID: AB_10673863
Rabbit-Anti-mouse Rictor (H-11)	Santa Cruz Bi	sc-271081; RRID: AB_10611167

(*Continued on next page*)

Continued

REAGENT or RESOURCE	SOURCE	IDENTIFIER
tetramethyl rhodamine B isothiocyanate-phalloidin	SIGMA	P1951; RRID: AB_2315148
Alexa Fluor 555 goat anti-mouse Ig	Biolegend	405324; RRID: AB_2563179
FITC Donkey anti-rabbit IgG	Biolegend	406403; RRID: AB_893531
Hexokinase 1	Abcam	ab65069; RRID: AB_1140844
HK2	Abcam	ab76959; RRID: AB_2248229
Mouse anti-Human CD3-Alexa Fluor 700	eBioscience	56-0038-80; RRID: AB_906222
Mouse anti-Human CD4-APC	BD Biosciences	555349
Mouse anti-Human CD25-PerCP Cyanine 5.5	eBioscience	45-0259-41; RRID: AB_10717820
Mouse anti-Human CD127-PE	eBioscience	12-1278-42; RRID: AB_10717663
Mouse anti-Human CD152 (CTLA-4)-BV786	BD Biosciences	563931
Mouse IgG2a, κ Isotype Control-BV786	BD Biosciences	563732
Mouse anti-Human CD357(AITR/GITR)-PE-eFluor 610	eBioscience	61-5875-41; RRID: AB_2574625
Mouse IgG1 K Isotype Control PE-eFluor 610	eBioscience	61-4714-80; RRID: AB_2637443
Mouse anti-Human CD69-PECy7	eBioscience	25-0699-41; RRID: AB_1548723
Mouse anti-Human CD45RA-FITC	BD Biosciences	555488; RRID: AB_395879
Mouse anti-Human CD197 (CCR7)-PE	BD Biosciences	552176; RRID: AB_394354
Mouse anti-Human Ki67-eFluor 450	eBioscience	48-5699-41; RRID: AB_10804032
Mouse anti-Human FoxP3-APC	eBioscience	17-4777-41; RRID: AB_2573208
Chemicals, Peptides, and Recombinant Proteins		
ProLong Gold Antifade	LifeTechnologies	P36930
Type IV Collagenase	Sigma,	Cat# C5138
trypsin/ (EDTA)	GIBCO	Cat# E7889
DMEM	GIBCO,	Cat# 11966-025
10% FBS	Seralab,	Cat# A210009
Dulbecco'sModified Eagle media (DMEM)	GIBCO	Cat# 41966-052
glutamine	GIBCO	Cat# 250-30
2-Mercaptoethanol (2-ME)	GIBCO	Cat# 31350-010
sodium pyruvate	GIBCO,	Cat# 11360-039
HEPES	GIBCO	Cat# 15630-056
non-essential amino acids	GIBCO,	Cat# 11140-050
trypsin/EDTA	GIBCO	Cat# T4049
murine IFN-γ	PeproTech	Cat# 315-05
Red blood cell lysis buffer	Sigma-Aldrich,	Cat# R7757
RPMI 1640 medium	GIBCO	Cat# 21875-034
GMCSF hybridoma	Dr. Jian-Guo Chai	NA
Murine TNF alpha	Peprotech	Cat# 315-01A
Zymosan	Sigma-Aldrich	Cat# z4250
mitomycin C	Sigma-Aldrich	Cat# M4287
Recombinant human IL-2	Roche	Cat# 10799068001
Recombinant murine CCL22	Peprotech	Cat # 250-23
succinimidyl ester dyes CFSE	Invitrogen	Cat# C1157
PKH26	Sigma-Aldrich	Cat# PKH26GL-1KT
DDAO-SE	Invitrogen	Cat# C34553
OCT	Thermo Fisher Scientific	Cat# 12678646
glucose free T cell medium	GIBCO	Cat# 11879-020
6-NBDG	Life Technologies,	Cat# N23106
RNeasy Mini Kit (50)	QIAGEN	Cat No./ID: 74104

(*Continued on next page*)

Continued

REAGENT or RESOURCE	SOURCE	IDENTIFIER
iQ SYBR Green Supermix	Biorad	#1708880
High-Capacity RNA-to-cDNA Kit	Life Technologies,	4387406
TaqMan human L 750 uL 80X – assay ID: C___2862880_1_	Applied Biosystem	4351374
TaqMan MasterMix 50 ML	Applied Biosystem	4371357
4–20% Mini-PROTEAN TGX Precast Protein Gels	Biorad	#4561096
Recombinant Mouse ICAM-1-Fc Chimera	Biolegend	553004
Recombinant human MIP-3β (CCL19)	Peprotech	300-29B
Recombinant human Exodus-2 (CCL21)	Peprotech	300-35
Recombinat human IL-2	Peprotech	200-02
Anti-Human CD3 Purified	eBioscience	14-0039-82
Anti-Human CD28 Purified	eBioscience	14-0289-82
1-step Fix/lyse solution	eBioscience	00-5333-54
UltraComp eBeads	eBioscience	01-2222-42
Ficoll-Plaque PREMIUM	GE-Healthcare	17-5442-03
Critical Commercial Assays		
Dynabeads FlowComp Mouse $CD4^+CD25^+$ Treg Cells Kit	Invitrogen	Cat#11463D
XF assay medium	Agilent Technologies	Cat# 102365-100
Seahorse XF Cell Mito Stress Test Kit	Agilent Technologies	103015-100
Seahorse XF Glycolysis Stress Test Kit	Agilent Technologies	103020-100
Anti-Mouse/Rat Foxp3 Staining Set APC	eBioscience	77-5775-40
Foxp3 / Transcription Factor Staining Buffer Set	eBioscience	00-5523-00
FlexiGene DNA kit	QIAGEN	51206
$CD4^+CD25^+$ Regulatory Tcell isolation kit, human	Miltenyi Biotec.	130-09-301
Experimental Models: Cell Lines		
Primary microvascular endothelial cells	NA	(Marelli-Berg et al., 2000)
Bone marrow-derived dendritic cells	This paper	NA
$CD4^+CD25^+$ Treg cells	This paper	NA
HEK293T	ATCC	CRL-11268
$CD4^+$ effector T primary cells	This paper	NA
Experimental Models: Organisms/Strains		
C57BL/6 mice	The Jackson laboratory	000664
CBA/Ca mice	The Jackson laboratory	000654
BALB/c mice	The Jackson laboratory	000651
Foxp3-GFP (Foxp3-IRES-EGFP) genetically targeted mice	Dr B Malissen	NA
$Cd28^{Y170F}$	Dr Klaus Okkenhaug	(Okkenhaug et al., 2001)
Oligonucleotides		
Glucokinase (hexokinase 4) primer: F:CAACTGGACCAAGGGCTTCAA; R:TGTGGCCACCGTGTCATTC	this paper	NA
Glut1: F:CACTGTGGTGTCGCTGTTTG; R:ATGGAATAGGACCAGGGCCT	this paper	NA
Hexokinase I: F:ATGATCGCCGCGCAACTAC; R:AGAGCCGCATGGCATACAGA	this paper	NA
Hexokinase II: F:CCGTGGACTGGACAACCTCA; R:CGTCACATTTCGGAGCCAGA	this paper	NA
Rictor: F:TCCCTCTAAGTTCTCGGGGA; R:TTAATGGTCAGAAGCCCGGT	this paper	NA

(*Continued on next page*)

Continued

REAGENT or RESOURCE	SOURCE	IDENTIFIER
Glucokinase Regulator: F:CAGCGTGAGTTAAGCACCAA; R:TCAGTGATGGAGCACCTGAG	this paper	NA
Serpinb9: F:CAGAGTTGTTGTCAGGTGGC; R:CGACACATCATCTGCACTGG	this paper	NA
GAPDH: F:AGAACGGGAAGCTTGTCATCA; R:GACCTTGCCCACAGCCTTG	this paper	NA
CCR4: F:TGGTGGAGCTTGAAGTCCTT; R:GGACATGTCAGCCGAGTAGA	this paper	NA
CCR7: F:GGGCTGGTGATACTGACGTA; R:ACACAGGTAGACGCCAAAGA	this paper	NA
CD103: F:GGGTCCTACTTTGGCTCTGT; R:GTGTGTGTGCCAAGGAGAAG	this paper	NA
CD62L: F:GGGAACGAGACTCTGGGAAA; R:ACCACATACTGACACTGGGG	this paper	NA
CD69: F:AAGGACCATGGCACCAGTAT; R:AGGTAGCAACATGGTGGTCA	this paper	NA
CXCR3: F:GGGGTCTCTGTCTGCTCTTT; R:CCTCATAGCTCGAAAACGCC	this paper	NA
CD11a: F:TCCGGAAAGTGGAGATGC T; R:GAAGTCTTCCCAGGAGCTGT	this paper	NA
CD49d: F:AGCCGTTGGTGCATTTCAAT; R:TGTAGCCTGGGACCTCTTTG	this paper	NA
Recombinant DNA		
pLKO.1 target gene set Gck	Sigma	TRCN0000012401
pLKO.1 target gene set Raptor	Sigma	TRCN0000077472
pLKO.1 – scramble shRNA	Addgene	Plasmid #1864
pLKO.1 target gene set Rictor	Sigma	TRCN0000123394
pMD2.G	Addgene	Plasmid #12259
pRSV-Rev	Addgene	Plasmid #12253
pMDLg/pRRE	Addgene	Plasmid #12251
Software and Algorithms		
Graphpad prism	Graphpad	http://www.graphpad.com
SPSS version 21	IBM Corporation	https://www.ibm.com/software/it/analytics/spss/
Flow Jo_v10	FlowJo	http://www.flowjo.com/
Microscopy Imaging software	AxioVision Rel.4.8	http://www.zeiss.com
ImageJ	ImageJ	https://imagej.nih.gov
Confocal microscopy	Leica LAS software	NA
Adobe Photoshop	Adobe systems	NA
NovoExpress	Acea Bioscience, Inc.	https://aceabio.com/products/novocyte/

CONTACT FOR REAGENT AND RESOURCE SHARING

Further information and requests for reagents may be directed to, and will be fulfilled by the corresponding author Federica Marelli-Berg (f.marelli-berg@qmul.ac.uk).

EXPERIMENTAL MODEL AND SUBJECT DETAILS

Ethical statement

Human blood was obtained from healthy donors according to ethical approval from the Università degli Studi di Milano (Cholesterol and Health: Education, Control and Knowledge – Studio CHECK [SEFAP/Pr.0003] – reference number Fa-04-Feb-01). All *in vivo* experiments were conducted with strict adherence to the Home Office guidelines (PPL 70/7443) following approval by the Queen Mary University of London Ethics committee.

Mice

All mice used in the experiments of this study were 7-11 weeks. C57BL/6, BALB/c and CBA/Ca mice were purchased from Charles River (UK). The *Foxp3-GFP* (Foxp3-IRES-EGFP) genetically targeted mice on the C57BL/6 background were kindly provided by Dr B Malissen (Centre d'Immunologie de Marseille-Luminy, Marseille, France). The *Cd28*^{Y170F} genetically targeted mice on the C57BL/6 background were provided by Dr K Okkenhaug (Babraham Institute). Excised secondary lymphoid organs from 4 week-old *Ctla-4*$^{-/-}$ mice (of H-2u haplotype) were provided by Prof D Wraith (University of Birmingham).

Isolation of microvascular endothelial cells

Murine lung microvascular endothelial cells were isolated as previously described (Marelli-Berg et al., 2000). Mouse lungs were diced into 2-3mm^3 blocks, washed in phosphate buffered saline (PBS; Sigma-Aldrich, Cat# D8537) and digested in a solution containing 0.5mg/ml Type IV Collagenase (Sigma, Cat# C5138) for 30 minutes in a humidified incubator maintained at 37°C. A 70μm cell strainer (Fisher scientific, Cat# 22363548) was then used to remove undigested tissue while the digested tissue was collected and centrifuged at low rpm (< 250 g). The supernatant was aspirated and further digested in trypsin/ (EDTA) (GIBCO, Cat# E7889) at 37°C for 5 minutes to create a uniform cell suspension. The cell suspension was then washed with PBS at 300 g and resuspended in DMEM (GIBCO, Cat# 11966-025) containing 10% FBS (Seralab, Cat# A210009). The cells were then seeded in 2% gelatinated (Sigma-Aldrich, Cat# 1393) 25 cm^2 culture flasks (Helena biosciences, Cat# 90026) for 24 hours. After 24 hours, non-adherent cells were removed by washing with warm PBS and complete EC medium (mentioned below) was added to the culture.

EC culture

EC medium consisted of Dulbecco's Modified Eagle media (DMEM, GIBCO, Cat# 41966-052) supplemented with 2 mM glutamine (GIBCO, Cat# 250-30), 50 IU/mL penicillin (GIBCO, Cat# 15140-122), 50 μg/mL streptomycin (GIBCO, Cat# 15140-122), 50 μM 2-Mercaptoethanol (2-ME) (GIBCO, Cat# 31350-010), 1mM sodium pyruvate (GIBCO, Cat# 11360-039), 20mM N-2-hydroxyethylpiperazine-N'-2-ethane sulfonic acid (HEPES) (GIBCO, Cat# 15630-056), 1% non-essential amino acids (GIBCO, Cat# 11140-050), 20% FCS and 150 μg/ml EC growth supplement (Sigma-Aldrich, Cat# E0760). Medium was replaced every 48 hours. When confluent, cells were detached with trypsin/EDTA (GIBCO, Cat# T4049) and passaged.

For functional assays, ECs were used between passages 2 and 8 and treated with 600 U/mL murine IFN-γ (PeproTech, Cat# 315-05) for 48 to 72 hours prior to use in experiments.

Isolation of bone marrow-derived Dendritic Cells (BMDCs)

Bone marrow(BM)-derived DCs were obtained from WT BALB/c (H2-d) mice. Femurs and tibias from 7–to-10-week-old female mice were removed and BM cells were flushed out with PBS using a 27-gauge needle (Becton Dickinson, Cat# 302200). Red blood cells were lysed from the cell suspension with lysis buffer (Sigma-Aldrich, Cat# R7757). BM cells (5x10^6) were seeded per well in a 6 well plate (Helena bioscience, Cat# 92006) in DC medium as described below.

Culture of Dendritic cells

Bone marrow-derived dendritic cells were cultured in RPMI 1640 medium (GIBCO, Cat# 21875-034) supplemented with 10% FCS, 2mM glutamine, 50 IU/mL penicillin, 50 μg/mL streptomycin, 50 μM 2-ME and 2% murine granulocyte-macrophage colony stimulating factor (GM-CSF) obtained from the supernatant of the GMCSF hybridoma (gift from Dr. Jian-Guo Chai, Imperial College, London, UK). Cells were cultured at 37°C in the presence of 5% CO_2. On days 3 and 5, fresh culture medium was added to the plates.

For Treg-DC cell co-cultures, immature BMDCs were collected and used on day 6 of culture. For functional assays, immature DCs were matured overnight with 100ng/ml lipopolysaccharide (LPS) (Invivogen, Cat# tlrl-3pelps) and were used between day 7-10 post-isolation.

Culture of H2-d allospecific Treg cells

CD4$^+$CD25$^+$ Treg cells were isolated from spleen and lymph nodes using Dynabeads® FlowComp Mouse CD4$^+$CD25$^+$ Treg Cells Kit (Invitrogen Dynal, Cat#11463D). For extremely high purity of Treg cells (> 99%), CD4$^+$CD25$^+$Foxp3$^+$ cells were obtained from Foxp3-GFP reporter mice through Fluorescence-activated Cell Sorting. For expansion, Treg cells isolated from C57BL/6 (H2-b) mice were stimulated weekly with either irradiated or mytomycin C (Sigma-Aldrich, Cat# M4287)-inactivated immature BALB/c-derived (H2-d) DCs at a ratio of 5:1 (Treg:DC) (Fu et al., 2014). The co-cultures were maintained in complete T cell medium supplemented with 10U/ml IL-2. Cells were harvested and seeded at an optimal density of 1.5x10^6 Treg cells per well of a 24-well tissue culture (Helena bioscience, Cat# 92024) plate each week. The percentage of CD4$^+$Foxp3$^+$ cells after two weeks of culture was greater than 95%. For use in functional assays, Treg cells were used 6-8 days after stimulation.

Antibody-mediated T cell activation

Activated T cells were obtained by polyclonal stimulation of LN cells with plate-bound anti-CD3 (1 μg/ml, eBiosciences, Cat# 16-0032-85) and plate-bound anti-CD28 (5 μg/ml, eBiosciences, Cat# 16-0281-86) in complete T cell medium supplemented with 20 U/ml recombinant IL-2 (Roche, West Sussex, UK) for 7 days at 37°C. Antibody coating of tissue culture plates was performed by incubating antibodies in 200 μL of Tris buffer (pH 8.5) at 37°C for 1 hour.

METHOD DETAILS

Lymphocyte trans-endothelial migration and chemotaxis assays

Primary microvascular ECs treated with IFN-γ for 48–72 h were seeded ($3x10^4$) and cultured on 2% gelatin-coated Transwell inserts (diameter, 6.5 mm) containing 3-μm pore size (Costar, Cat# CLS3472-48EA) polycarbonate membranes in EC medium for 16 h to from a monolayer. T cells ($5x10^5$) resuspended in migration medium (RPMI 1640 supplemented with 2% fetal bovine serum) were added to each insert and left to migrate through the monolayer; the well volume was also replaced with fresh migration media. The number of migrated T cells was determined by a hemocytometer counting of the cells present in the well media at different time points over a 24-h period. To measure chemotaxis, T cells were seeded onto Transwell bare-filter tissue culture well inserts (diameter, 6.5 mm) with 5- or 3-μm pore size (Costar, Cat# CLS3421-48EA) polycarbonate membranes and chemokine-containing migration medium was placed in the bottom of the well. The number of migrated cells was determined by a hemocytometer.

Assessment of Treg cell apoptosis

Apoptosis of Treg cells treated with increasing doses of TNFα (5 and 50 ng/ml, PeproTech,INC, Cat# 315-01A) or heat was measured using Annexin V-FITC Apoptosis Detection Kit (Abcam, Cat#ab14085). Cells were subsequently analyzed using flow cytometry.

Induction of CD28, CTLA-4 and LFA-1 signaling

Induction of CD28 and CTLA-4 signaling by antibody stimulation was performed as previously described (Schneider et al., 2005; Wells et al., 2001). To induce co-stimulatory signals via CD28 and CTLA-4 co-receptors for functional assay, cells were incubated with antibodies targeting the functional domains of the co-receptors. To induce CD28 signaling, T cells were treated with a mixture of hamster anti-mouse CD28 (5 μg/$5x10^6$ cells) (clone: 37.52, Bio-Rad, Cat# MCA1363) and goat anti-hamster immunoglobulin (Ig) (2.5 μg/$5x10^6$ cells) (Bio-Rad, Cat# STAR104) for different time points as described in each figure separately. Similarly, CTLA-4 signaling was achieved by incubating T cells with a mixture of hamster anti-mouse CTLA-4 (5 μg/$5x10^6$ cells) (clone: UC10-4F10-11, Becton Dickinson, Cat# 553718), and goat anti-hamster immunoglobulin (Ig) (2.5 μg/$5x10^6$ cells) (Bio-Rad, Cat# STAR104). A hamster IgG isotype control was used to observe any non-specific effects of the antibody stimulation (Bio-Rad, Cat# MCA2356). To induce LFA-1 signaling, cells were incubated with 2 μg/$5x10^6$ cells recombinant mouse ICAM-1-human IgG Fc chimeras (2 μg/ml, R&D Systems, Cat# 796-IC-050) or human IgG-Fc fragments (R&D Systems, Cat# 110-HG) as a control – either plastic-bound or ligated with a mouse anti-human IgG (1 μg/ml, MK1A6, Bio-Rad Cat# MCA647G) - for different time points as described in each figure separately. T cells were washed in PBS prior to use in the experiments.

Fluorescent labeling of viable T cells

For labeling T cells with fluorescent probes, T cells were washed with PBS, counted and resuspended in PBS at a final concentration of 10^7/ml. If necessary, dead cells were removed using density gradient centrifugation with Ficoll-Paque prior to re-suspension. Labeling of T cells with PKH26 (Sigma-Aldrich, Cat# PKH26GL-1KT), a cell linker dye for cell membranes was performed using manufacturer instructions. PKH26 was added at a final concentration of 5μM, and the cells were incubated at room temperature for 5 minutes. The reaction was inactivated by adding an equal volume of FBS to the cell suspension and the cells were washed in PBS containing 10% FBS for 10 minutes. Labeling of T cells with succinimidyl ester dyes CFSE (Invitrogen, Cat# C1157) or DDAO-SE (Invitrogen, Cat# C34553) was performed by incubating the T cells in PBS containing final concentration of 3.3 μM CFSE or 1.3 μM DDAO-SE for 10-15 minutes at room temperature. The reaction was terminated by adding equal volume FBS and the cells were then washed with PBS containing 10% FBS for 10 minutes.

T cell recruitment in the peritoneum

To observe *in vivo* recruitment of T cells we used a previously described model (Mirenda et al., 2007). Either PKH26 or CFSE or DDAO-SE-labeled T cells (10^7) were injected intravenously (i.v.) into mice that hd received IFN-γ (600U) via intraperitoneal injection (i.p.) 48 to 72 hours earlier. Labeled T cells recovered via peritoneal lavage were analyzed 16 hours later using flow cytometry. In addition, localization of Treg cells to the spleen, where entry occurs in a passive manner, was analyzed to ensure that similar numbers/proportion of labeled cells were injected or co-injected in all recipients (internal control).

Zymosan-induced peritonitis

On day 0, mice were given intraperitoneal injections of Zymosan (1 mg/mouse, Cat# 4250 SIGMA) in sterile saline solution to induce peritonitis. Mice were sacrificed 72 hours post-injection and tissue samples obtained for flow cytometry analysis.

Widefield deconvolution fluorescence microscopy

Tissues samples were excised, embedded in Optimal Cutting Temperature compound (OCT; Thermo Fisher Scientific, Cat# 12678646), snap-frozen and stored until analysis. Frozen tissue sections were laid onto Polysine coated microscope slides (VWR International, Cat# 47100), air-dried and then fixed with ice cold acetone (Sigma, Cat# 534064) for 10 min. Tissue sections were washed in PBS, blocked with serum for 3 hours and stained using mentioned primary antibodies at 4°C for 24 h. Excess antibody was washed away with PBS and tissues were stained with indicated secondary antibodies along with DAPI (4',6-diamidino-2-phenylindole) (Invitrogen/LifeTechnologies, Cat# D1306) for 30 min at room temperature. Slides were washed, mounted in ProLong Gold

Antifade Reagent (Invitrogen/Life Technologies, Cat# P36930) and visualized using a Zeiss Z1 fluorescence microscope (Carl Zeiss, UK) equipped with an AxioCam MRm Cooled monochrome digital camera and an Apotome 2 Imaging unit. Images were acquired using a Plan Apochromat 20x/0.8 NA objective and Axiovision software version 4.8 (Carl Zeiss, UK). For staining, Treg cells were cultured in R10 medium and fixed with 3.7% formaldehyde. After fixing, they were stained with anti- GCK, anti-Na,K-ATPase and 1 ng/ml tetramethyl rhodamine B isothiocyanate–conjugated phalloidin (Sigma-Aldrich Cat# P1951) for 30 min at 37°C and respectively. This was followed by secondary antibodies Alexa Fluor® 555 goat anti-mouse Ig (Biolegend Cat# 405324) and FITC Donkey anti-rabbit IgG (minimal x-reactivity) Antibody (Biolegend 406403). Coverslips were extensively washed, air-dried, and mounted in Vectorshield mounting medium for fluorescence with DAPI (Vector Laboratories Cat# z0603) on glass slides.

Confocal microscopy

Cells were allowed to adhere onto poly-L-lysine coated coverslips and fixed in 4% paraformaldehyde (Thermo Fisher Scientific, Cat# 28906) for 5-10 minutes at room temperature. Where mentioned, permeabilization was carried out using 0.2% Triton X-100 (Sigma-Aldrich, Cat# X100-500ML) in PBS for 5 minutes. Cells were then washed in PBS, blocked in blocking buffer (PBS containing 0.1% Fish skin gelatin; Sigma-Aldrich, Cat# G7765) and 1% serum of the species giving rise to secondary antibodies) for 3-6 hours and then stained with appropriate primary antibodies at 4°C for 16 hours in the dark. Following staining, cells were washed again and stained with corresponding secondary antibodies and DAPI for 30 minutes at room temperature. After multiple PBS washes coverslips were mounted onto slides using ProLong Gold Antifade (Invitrogen/Life Technologies, Cat# P36930) and then examined using a Leica SP5 confocal microscope equipped with a 63 × 1.4 NA objective. Confocal images and Z stacks were acquired and analyzed by Leica LAS software. Repositioning of scale bars and image layouts were prepared using Adobe Photoshop (Adobe Systems). All images in a group were treated equally.

In vitro 6-NBDG uptake assay

Freshly isolated or cultured T cells were washed in PBS and resuspended in glucose free T cell medium (GIBCO, Cat# 11879-020) containing various mentioned signaling antibodies and incubated for 45 minutes at 37°C with 5% CO2. A final concentration of 400 μM 6-NBDG (Life Technologies, Cat# N23106) in glucose free T cell medium was then added to the cells and the cells were further incubated for an additional 10-15 minutes. Finally, the cells were washed twice with warm PBS and resuspended in flow cytometry buffer and placed on ice. Immediate analysis was performed using flow cytometry to observe fluorescence uptake by the T cells.

In vitro 6-NBDG uptake assay (human studies)

Freshly isolated $CD3^+$ T cells were washed in PBS and cultured 10^6/mL in R2 (RPMI 1640 supplemented with 2% fetal bovine serum) with recombinant CCL19 and CCL21 (200 ng/mL - Peprotech Cat#300-29B and 300-35) at 37°C with 5% CO_2. A final concentration of 400 μM 6-NBDG (Life Technologies, Cat# N23106) was added to the cells and incubated for 0, 15, 30 and 60 minutes. Finally, the cells were washed twice with warm PBS, stained for $CD4^+$ T cells and Treg and placed on ice. Immediate analysis was performed using flow cytometry to observe fluorescence uptake by Treg cells.

In vivo 6-NBDG uptake assay

To measure glucose uptake activity of T cells *in vivo*, PKH26 labeled T cells ($3x10^6$) were injected i.p. into mice. A second i.p. injection of 6NBDG (400 μM in Sterile water) was given to the mice immediately afterward. After a 1-hour period, the mice were sacrificed and the mesenteric (draining) lymph nodes and spleen collected for analysis by flow cytometry. Widefield microscopy of the peritoneal membranes was performed to observe influx of labeled T cells into the peritoneal membrane. $PKH26^+$ T cells infiltrating the membranes were further analyzed for 6NBDG uptake (green fluorescence) using image analysis software ImageJ. The number of labeled cells in 10x magnification field views images was counted manually to determine differences in T cell infiltration.

Measurement of ECAR and OCR

Real time bioenergetics analysis of extracellular acidification rates (ECAR) and oxygen consumption rates (OCR) of T cells subjected to antibody stimulation was performed using the XF analyzer (Seahorse biosciences). T cells were cultured in serum free, unbuffered XF assay medium (Seahorse biosciences, Cat# 102365-100) for 1 hour. The cells were then seeded ($6x10^5$/well) into the seahorse XF24 cell plates for analysis. Perturbation profiling of the use of metabolic pathways by T cells was achieved by the addition of oligomycin (1 μM), FCCP (1 μM), Antimycin A (1 μM), rotenone (1 μM), D-glucose (10mM), 2-Deoxy-D-glucose (2DG, 50mM; all from Seahorse biosciences, Cat# 103020-100 and 103015-100). Experiments with the Seahorse system were done with the following assay conditions: 2 min mixture; 2 minutes wait; and 4–5 min measurement. Metabolic parameters were calculated. Experiments were done in at least triplicate wells.

Surface staining

For surface staining, cells were resuspended (10^7/ml) and stained with flurochrome- conjugated antibodies in 100 μL of Flow cytometry buffer made of PBS containing 0.1% sodium azide (Sigma-Aldrich, Cat# S2002-25G) and 1% FBS at 4°C for 30 minutes. CCR7 antibody staining was performed at 37°C for 30 mins. Optimal antibody concentrations for staining were calculated based on manufacturer instructions. Following staining, cells were washed and resuspended with flow cytometry buffer and analyzed

immediately. Alternatively, for delayed analysis, cells were fixed in fixation buffer (flow cytometry buffer containing 1% Formaldehyde, Sigma-Aldrich, Cat# 15,812-7)) for 30 minutes at 4°C, washed and stored in flow cytometry buffer at 4°C. The table below indicates the fluorescent antibodies that were used in this study.

Intracellular staining

For intracellular Foxp3 staining, eBioscience Anti-Mouse/Rat Foxp3 Staining Set APC (clone FJK-16S, Thermo Fisher Scientific Cat# 17-5773-82) kit was used. Cells were resuspended (10^7/ml) and stained with surface antigens as mentioned above and then fixed/permeabilized for 30 minutes at 4°C using Fixation/Permeabilization working solution made from mixing 1 part of the fixation/permebilization concentrate (eBioscience, Cat# 00-5123) to 3 parts of the fixation/permebilization diluent (eBioscience, Cat# 00-5223). The cells were then washed twice in 1X permeabilization buffer (eBioscience, Cat# 00-8333) and stained with fluorochrome conjugated-Foxp3 antibody in 1x permeabilization buffer for 30 minutes at 4°C. A final wash with 1x permeabilization buffer was performed and the cells were then centrifuged and resuspended in 200ul of flow cytometry buffer. For T cell proliferation studies, Treg cells were stimulated with immature BALB/c DCs. 3 hours later, Treg cells were fixed and permeabilized with ice cold 70% ethanol before staining for proliferating cell nuclear antigen (PCNA, clone PC10, BioLegend Cat# 307908).

In vitro AKT phosphorylation (human studies)

Freshly isolated concentional $CD4^+CD25^-$ T cells (Tconv) and $CD4^+CD25^+$ (Treg) T cells were washed in PBS and cultured 5×10^6/mL in R2 (RPMI 1640 supplemented with 2% fetal bovine serum). 0.5×10^6 $CD4^+CD25^-$ (Tconv) and $CD4^+CD25^+$ (Treg) were plated in 96-well plate and stimulated for 15 minutes or not with chemokines CCL19 and CCL21 (1 μg/mL - Peprotech Cat# 300-29B and 300-35) at 37°C with 5% CO_2. Cells were immediately fixed to stop stimulation with 2% formaldehyde for 10 minutes at RT in the dark. Cells were washed and resuspended in 100% ice-cold methanol and incubated for 30 minutes on ice. Subsequently, cells were washed twice with PBS 2%FBS and stained for pAKT-s473 (eBioscience, Cat# 17-9715-41) for 30 minutes at 4°C in the dark. Cells were washed, resuspended in PBS 2%FBS and immediately analyzed by flow cytometry.

Western Blotting and coimmunoprecipitation

Whole-cell lysates were lysed in Nonidet P-40 lysis buffer [50 mM HEPES (pH 8.0), 350 mM NaCl, 1% Nonidet P-40, 1 mM EDTA, 1 mM Na3VO4, 1 mM NaF, 20 mM glycerol-2-phosphate, 1 mM PMSF, 1 mM DTT, 10 μg/mL aprotinin, 10 μg/mL leupeptin, and protease inhibitor cocktail (Roche Cat# 11836145001). Equivalent amounts of protein as determined by standard Bradford assay (Bio-Rad Cat# 5000001) were separated by SDS/PAGE and transferred to nitrocellulose membrane (GE Healthcare Life Sciences Cat# 10600002). Membranes were blocked for 2 h at room temperature in 5% milk/TBS-Tween 20 (Sigma Cat# P1379) and were incubated overnight at 4°C with the primary antibodies listed below. HRP-conjugated secondary antibody (1:5000; Amersham Bioscience Cat# NA934) was subsequently added. Films were then developed. The intensity of the bands was quantified using ImageJ (NIH). For coimmunoprecipitation experiments, cell extracts were prepared in RIPA buffer. 250 μg of total protein extract was first precleared with Protein G–Agarose beads (Sigma Cat# P3296) for 1 hour at 4°C, incubated with 5 μg of anti-GCK Ab (Santa Cruz Biotechnology Cat# SC7908) overnight at 4°C and then with Protein G beads for another 16hrs at 4°C. The final pellet was resuspended in 10 mM Tris HCl, pH 7.4, supplemented with 1 mM PMSF and analyzed by western blot for B actin (Santa Cruz Cat# SC161).

Quantitative real time PCR (qRT-PCR)

Tissues were harvested and stored in RNA-later (QIAGEN Cat# 76104) at –80°C until processing. RNA was purified using Trizol reagent (Life Technologies Cat# 15596) according to the manufacturer's instructions and assessed for quality and quantity using absorption measurements. Reverse transcription was performed according to the manufacturer's instruction (Applied Biosystems Cat# 4374966). Gene expression analysis was done using SYBR Green Supermix (Biorad Cat# 1725120) in CFX connect light cycler (Biorad Cat# **1855200**). Expression was calculated using the ΔΔCt method (Livak and Schmittgen, 2001) and normalized to a housekeeping gene (GAPDH). Primers for qPCR were designed with the help of online tools (Primer 3Plus) using at least one exon junction-binding site per primer pair. The thermal cycling profile for amplification was 95°C for 10 min, followed by 40 cycles of 95°C for 15 s and 54°C for 1 min. Amplification was at 95°C for 10 min, followed by 40 cycles of 95°C for 15 s and 60°C for 1 min. To ensure the amplification specificity, the melting curve program was set as follows: 95°C for 15 s, 60°C for 1 min, and 95°C for 15 s, right after the PCR cycles. Experiments were done in triplicates.

Lentivirus Preparation for Gene Silencing

HEK293T cells were grown in 10cm cell-culture dishes to 70% confluence and were transfected with the above plasmids using the calcium phosphate method. The supernatant was harvested 48 and 72 h after transfection and was concentrated 100-fold in an ultracentrifuge. Aliquots were stored at −80°C. For transduction of Treg cells, cells were seeded in six-well plates and cultured in DMEM to 60%–70% confluence. Lentivirus was added to the cells in the presence of 5 μg/mL Polybrene (Sigma-Aldrich Cat# 107689), and the six-well plate was centrifuged at 2,300 rpm for 90 min at room temperature, followed by 8 h incubation at 37°C with 5% CO_2. Virus was removed 24 h later; T cells were washed twice with PBS and incubated for 24 h in complete DMEM (Life technologies, Cat# 1852730).

Study population

The Progressione della Lesione Intimale Carotidea (PLIC) Study (a sub-study of the CHECK study) is a large survey of the general population of the northern area of Milan (n = 2.606) (Baragetti et al., 2015; Lorenz et al., 2012; Norata et al., 2009; Norata et al., 2006), followed at the Center for the Study of Atherosclerosis, Bassini Hospital (Cinisello Balsamo, Milan, Italy). The Study was approved by the Scientific Committee of the Università degli Studi di Milano (“Cholesterol and Health: Education, Control and Knwoledge – Studio CHECK ((SEFAP/Pr.0003) – reference number Fa-04-Feb-01) in Febraury 4th 2001. An informed consent was obtained by subjects in accordance with the Declaration of Helsinki.

Genomic DNA was extracted using Flexigene DNA kit (QIAGEN, Milan, Italy). Genotyping for the p.Leu446Pro *GCKR* missense mutation was available on the entire population, using TaqMan allelic discrimination test. The experimental analysis was conducted on a subgroup of 16 subjects, eight Leu 446-*GCKR* and eight Pro 446-*GCKR* matched for age and gender.

Blood surface and intracellular staining (human studies)

For surface staining, 100μL of whole blood were stained with flurochrome-conjugated antibodies in 50 μL of MACS buffer made of PBS containing, 2% FBS and 2μM EDTA at RT (room temperature) for 30 minutes in the dark. Optimal antibody concentrations for staining were calculated based on manufacturer instructions. Following staining, red blood cells were lysed with 2 mL of 1-step fix/lyse solution (eBioscience, Cat#00-5333-54) for 20 minutes at RT, washed and resuspended with MACS buffer and analyzed immediately.

Alternatively, for intracellular staining, peripheral blood mononuclear cell (PBMCs) were isolated (as described below) and used for the staining (1-step fix/lyse solution is incompatible with some intracellular stainings). Cells were resuspended (10^7/mL) and stained in in 50 μL of MACS buffer with surface antigens. For intracellular Foxp3 and Ki67 staining, eBioscience Anti-Mouse/Rat Foxp3 Staining Kit was used (Cat#77-5775-40). Cells were fixed/permeabilized ON at 4°C using Fixation/Permeabilization working solution made from mixing 1 part of the fixation/permebilization concentrate to 3 parts of the fixation/permebilization diluent. Cells were then washed twice in 1X permeabilization buffer and stained with fluorochrome conjugated-Foxp3 and –Ki67 antibodies in 1x permeabilization buffer for 30 minutes at 4°C. A final wash with 1x permeabilization buffer was performed and the cells were then centrifuged and resuspended in 200 μL of MACS buffer. The table above indicates the fluorescent antibodies that were used in this study.

PBMC isolation and $CD4^+CD25^+$ Treg cell purification (human studies)

For each subject, 30 mL of blood (supplemented with EDTA) were split in two falcon of 15 mL and spin for 12 minutes at 1000xg. Plasma was discarded and the interface between plasma and red blood cells, enriched in leukocytes and platelets (buffy coat), was carefully collected, diluted with cold PBS and stratified on 3 mL of Ficoll-Plaque™ PREMIUM (GE-Healthcare, Cat#17-5442-03). After centrifugation of 35 minutes at 250xg, PBMC layer was carefully collected and was 3 times with 10 mL of cold PBS at 180xg for 12 minutes to get rid of platelets. PBMC were counted and use for $CD4^+CD25^+$ Treg purification with $CD4^+CD25^+$ Regulatory T cell isolation kit, human (Miltenyi Biotec., Cat#130-09-301) according to manufacturer instructions. Purified $CD4^+CD25^+$ Treg or $CD4^+CD25^-$ Tconv cell were counted with a hemocytometer and used for migration and suppression assay.

Treg and Tconv cell migration assay (human studies)

300 μL of Treg and Tconv cells ($1x10^5$) of each subject were resuspended in migration medium (RPMI 1640 supplemented with 2% fetal bovine serum) and cultured on Transwell inserts (diameter, 6.5 mm) with 5-μm pore size (Costar, Cat# CLS3421-48EA) polycarbonate membranes. Cells were left to migrate versus migration medium or chemokines CCL19 and CCL21 (200 ng/mL - Peprotech Cat#300-29B and 300-35), placed in the bottom of the well, for 1, 2, 4 and 12 hours. The number of migrated cells was determined by a hemocytometer and data expressed as percentage of migration compared to cultured cells.

Suppression assay (human studies)

$CD4^+CD25^-$ Tconv cells were resuspended in MACS buffer (10^7/mL) and labeled with succinimidyl ester dyes CFSE (2μM - Invitrogen, Cat# C1157) for 10 minutes at RT in the dark. Cells were washed 3 times with MACS buffer and centrifuged at 360xg for 5 minutes. 96 well-plate U-bottom were coated with anti-human CD3 purified antibody (5 μg/mL - eBioscience, Cat#14-0039-82) for 1 hour at 37°C. Tconv were resuspended (10^6/mL) in complete medium (RPMI 1640 supplemented with 10% FBS, 1mM Na-Pyruvate, 10mM HEPES, 50 μM β-MeOH and pen/strep/glutamine) plus 50 U/mL of IL-2 (Peprotech; Cat#200-02) and 2 μg/mL of anti-human CD28 purified antibody (eBioscience, Cat#14-0289-82) and ($1x10^5$/100 μL) were plated. $CD4^+CD25^+$ Treg cells were washed and resuspended in complete medium and added to Tconv cells according to the following proportions (Tconv:Treg): 1:1, 1:0,5, 1:0,25 and 1:0 by performing serial dilution of Treg cells with complete medium in a 96-well plate. The plate was then spun 1 minute at 120 g and incubated at 37°C for 4 days. Cells were then collected and for each subject the percentage of proliferated cells in the presence of Treg cells was compared to the condition of Tconv:Treg cells 1:0 (100% proliferation).

QUANTIFICATION AND STATISTICAL ANALYSIS

The qPCR data were analyzed using the delta delta CT method by taking the CT values of the genes of interest from the house keeping gene following by normalization to the wild-type control sample. Results were done transported to prism before graphic presentation and statistical analysis.

Results are given as the mean per group ± SD. The data were analyzed using a two-tailed unpaired Student's t test and Mann-Whitney test. A p value of less than 0.05 was considered significant. Experimental datasets from the seahorse were analyzed using one-way ANOVA with Bonferroni correction or Kruskal-Wallis with Dunn's post-test to take into account of multiple comparisons. Where indicated 'n' represent the number of biological replicates. Human data were analyzed by ANCOVA (Analysis of Co-Variances) models between TT and CC genotypes of the rs1260326 GCKR polymorphisms (adjusting by age and gender). In supplemental table variables are presented as mean (standard deviations, SD) if normally distributed or as median (Inter-Quartile Range, IQR) if non normally distributed (Shapiro-Wilk test). t test to compare normally distributed variables and U-Mann Whitney for non-normally distributed variables were performed (p values for each variables are reported; p less than 0.05 are significant). Grubb's test for outliers detection was performed for each variables.

For human results, data are reported as the mean per group ± SEM. The data were analyzed using a two-tailed unpaired Student's t test and Mann-Whitney test. A p value of less than 0.05 was considered significant.